SWECLIM
SWEDISH REGIONAL CLIMATE MODELLING PROGRAMME

SMHI

No 98, 2001

Reports Meteorology and Climatology

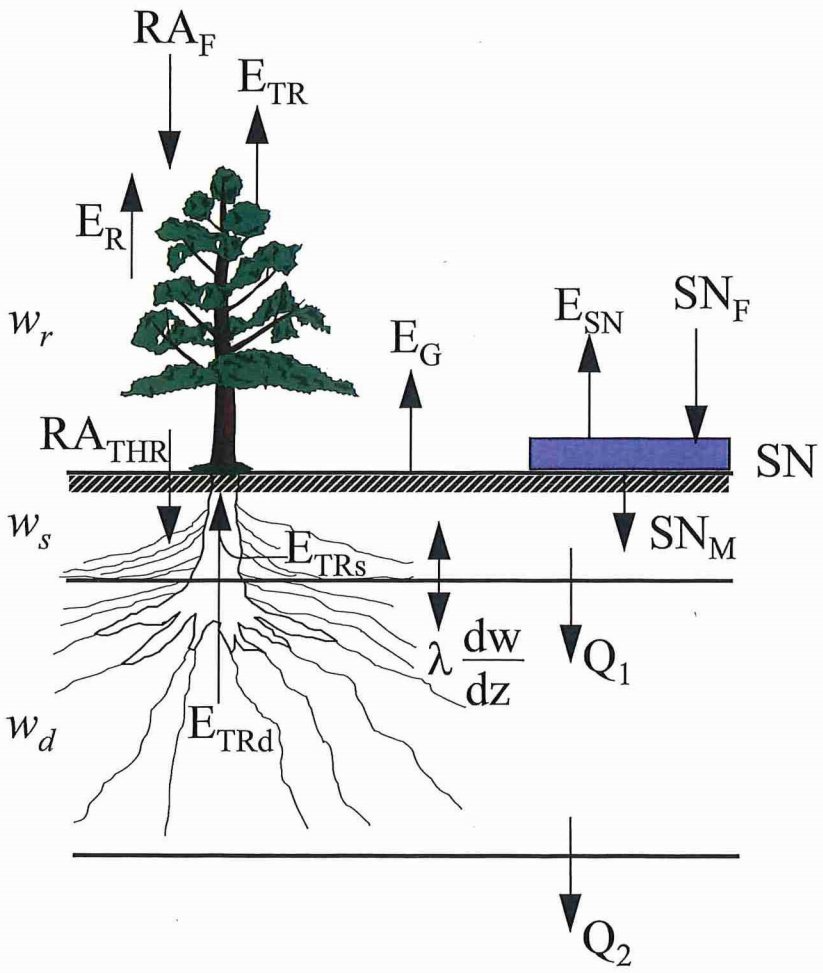

The land surface treatment for the Rossby Centre Regional Atmospheric Climate Model - version 2 (RCA2)

Björn Bringfelt, Jouni Räisänen, Stefan Gollvik, Göran Lindström, L. Phil Graham and Anders Ullerstig

Cover illustration: Evapotranspiration and moisture components used by RCA2.

RMK No. 98, Dec 2001

The land surface treatment for the Rossby Centre Regional Atmospheric Climate Model – version 2 (RCA2)

Björn Bringfelt, Jouni Räisänen, Stefan Gollvik, Göran Lindström, L. Phil Graham and Anders Ullerstig

Rossby Centre, SMHI

Report Summary / Rapportsammanfattning

Issuing Agency/Utgivare	Report number/Publikation
Swedish Meteorological and Hydrological Institute S-601 76 NORRKÖPING Sweden	RMK No. 98
	Report date/Utgivningsdatum December 2001

Author (s)/Författare

Björn Bringfelt, Jouni Räisänen, Stefan Gollvik, Göran Lindström, L. Phil Graham and Anders Ullerstig

Title (and Subtitle/Titel

The land surface treatment for the Rossby Centre Regional Atmospheric Climate Model – version 2 (RCA2)

Abstract/Sammandrag

A new version of the land surface scheme has been completed and is now applied in comparative tests of version 2 of the Rossby Centre Regional Atmospheric Climate Model (RCA2) using analysed fields from the ECMWF reanalysis project (ERA). The scheme contains two soil layers and a vegetation layer. There are two prognostic temperatures, one covering the top soil layer plus vegetation and one for a second, deeper soil layer. There is also a third, bottom soil temperature relaxed to six-hourly ERA fields. For soil moisture there are two prognostic layers but no bottom relaxation is used. A hydrologically-based soil moisture model (beta model) is used to represent subgrid soil moisture variability. A hydrological snow model makes regard to subgrid temperature variability using a geographical database for variance of topography. There are equations for heat and moisture exchange between the two soil layers. Here the hydraulic and thermal properties depend on soil type and soil moisture. Transpiration flux transports moisture from both soil layers depending on a stomatal resistance of vegetation surfaces as function of daylight intensity, soil water deficit, fraction of frozen soil water, air temperature and water vapour pressure deficit in the air. A treatment of rainfall interception on vegetation is used, broadly following the ISBA model, with a vegetation layer storing intercepted water. Subgrid weighting of albedo, surface roughness and parameters for calculating surface resistance is made using a geographical database for area fraction of forest and open land. The leaf area index varies seasonally for short vegetation and for deciduous forest, but not for coniferous forest. A soil freezing/melting algorithm influencing soil temperature is used. Implicit methods are used for solving the equations of most surface variables. A summary of model results compared to observations, is given at the end of the report.

Key words/sök-, nyckelord

Land surface parameterization, regional climate modelling, HIRLAM, HBV

Supplementary notes/Tillägg	Number of pages/Antal sidor	Language/Språk
This work is a part of the SWECLIM programme.	40	English

ISSN and title/ISSN och titel

0347-2116 SMHI Reports Meteorology Climatology

Report available from/Rapporten kan köpas från:

SMHI
S-601 76 NORRKÖPING
Sweden

Contents

1 Introduction

The land surface schemes used for the different versions of the Rossby Centre Regional Atmospheric Climate Model (RCA) were originally developed on the basis of the former standard version 2.5 of HIRLAM (High Resolution Limited Area Model; Källén 1996). HIRLAM is a weather forecasting system in operational use and under continuous development in the international HIRLAM project participated in by Denmark, Finland, Iceland, Ireland, the Netherlands, Norway, Spain and Sweden. France also cooperates in the project.

The task of a land-surface scheme is to calculate the time tendencies of surface variables (e.g. soil temperature and moisture) while fulfilling both the energy and water balances at the land-atmosphere interface (see Viterbo 1996 for a review). The land-surface forecast variables in the scheme described here are surface temperature, deep soil temperature, surface soil moisture, deep soil moisture, rain water stored on vegetation canopy, snow depth (as water equivalent) and previous maximum snow depth.

The parameterization of soil temperature is much the same as in HIRLAM, but with modification for frozen soil moisture. The soil is divided into two active layers and a climatological bottom layer. The top soil layer and the vegetation layer are represented by only one common temperature. The climatological layer soil temperatures are based on 6-hourly values from GCM simulations or ERA fields (Gibson et al. 1997). For soil moisture there are only two layers and no relaxation to climatological values is made. Thermal and hydraulic and diffusivity, accounting for heat conduction and capillary moisture fluxes respectively, both depend on soil texture type and soil moisture. As in the original standard version, the surface scheme is used when the fraction of land plus ice in a grid square is greater than a fixed fraction, here 0.1 per cent. For this land plus ice surface there is one common value of surface temperature, deep temperature, snow depth, maximum snow depth and calculated fractional snow cover.

Important improvements in the present surface scheme are devoted to the hydrological cycle such as hydrology-based soil moisture, runoff, snow and a treatment of rainfall interception on vegetation. The subgrid land surface fraction is divided between forest and open land. Prescribed values for the forest and open land parts are used for albedo, surface roughness and parameters such as leaf area index used in calculating surface resistance. These values are weighted together for the whole grid land surface value with respect to the subgrid fractions of open land and forest. For the land, ice, and open water subgrid areas, flux aggregation is used, i. e. their subgrid surface fluxes are weighted. Time-step forecasts of surface variables are made using implicit solutions for time step centered averages.

In the three-dimensional model runs discussed toward the end of this report (Section 14), the soil scheme described below was used in version RCA2 of the Rossby Centre Regional Atmospheric Climate Model, which includes mainly the dynamic part and the

interface to the physics from the original HIRLAM code. Changes in other parts of the model physics will be outlined in Section 14.

2 The surface energy balance

In the land-surface treatment, the terms of the energy balance of the earth surface are used in the prognostic equation for the soil temperature. The most important fluxes to be discussed here are the net radiation flux, R_n, the sensible heat flux, H, and the latent heat flux, LE. R_n is weighted net radiation from the subgrid snow covered and snow free open land and forest areas. The vertical sensible heat flux and water vapour flux are calculated by flux-gradient relationships. The net downward energy flux at the surface (G), used in Eq. (51) (Section 7) for the common temperature T_s of the top soil layer and the vegetation is described by

$$G = R_n - H - LE - M_{eff} - P_{eff} \tag{1}$$

M_{eff} and P_{eff} are the heat contributions from snowmelt and melting/freezing precipitation, respectively. The sensible heat flux (Wm^{-2}) is written as

$$H = c_p \rho \frac{T_s - T_a}{r_a} \tag{2}$$

c_p and ρ are the air heat capacity and density, respectively. The same surface temperature T_s is used for the whole grid cell land area. T_a is temperature at the lowest model level. r_a is the grid cell aerodynamical resistance between the surface and the lowest model level. The stability functions for r_a are given by Louis et al. (1982).

3 Evapotranspiration components

The sensible heat flux, H, is formulated similarly for all types of surfaces, but the latent heat flux, LE, is formulated differently. LE depends on the characteristcs of the surface in question. Below, evapotranspiration will be expressed in kg m^{-2} s^{-1} omitting the latent heat of vaporization, L.

The different evapotranspiration components are illustrated in Fig. 1. Outside the growing season only soil moisture and snow cover control the evapotranspiration. During the growing season, the total evapotranspiration from the vegetation canopy is calculated as the sum of a transpiration part and an intercepted water part. The evaporation rate from the bare soil, E_G, transports moisture from the top soil layer. The transpiration components for dry vegetation, E_{TRs} and E_{TRd}, transport moisture from the top soil layer and the deep soil layer, respectively, assuming the same vegetation root density in both layers. E_R is the evaporation from the fraction, δ, of the foliage covered by intercepted water.

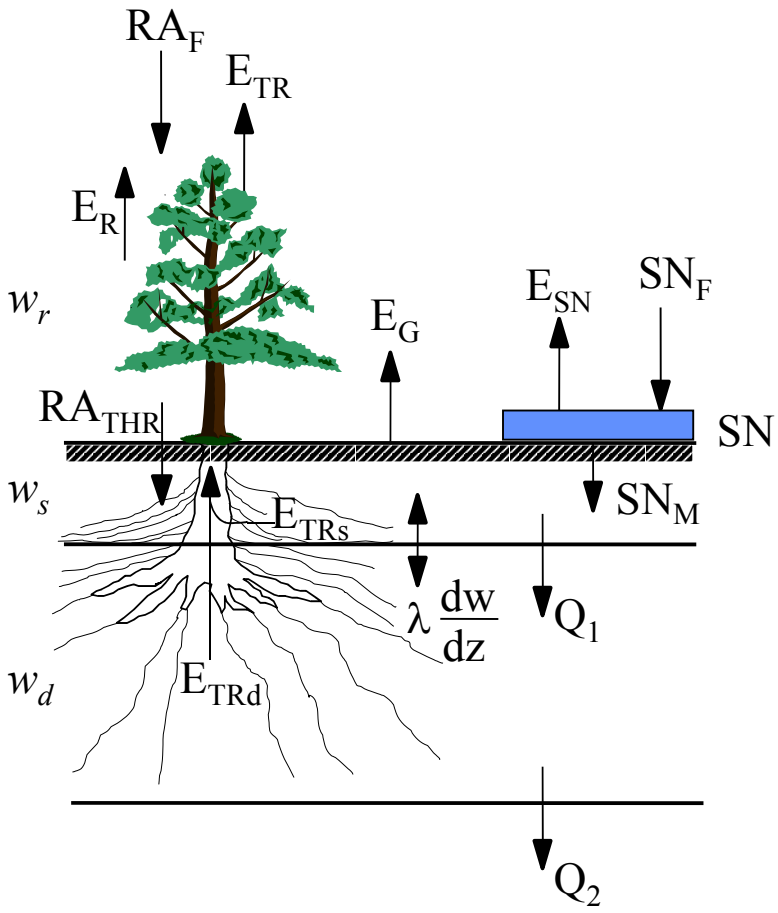

Figure 1. *Water flux and water storage components used by RCA2.*

As described below, the parameter values used for calculating the evapotranspiration components are weighted between typical values for forest and open land according to the fractional areas *frfor* and *fropl* of these area types. The total evapotranspiration rate *E* (used as input to the atmosphere and a loss from the land surface) is

$$
\begin{aligned}
E = \; & \\
& (E_R + E_{TR\delta}) \cdot [frfor + fropl \cdot (1 - frsn)\,] && \text{(canopy: interception+transpiration)} \\
& + E_G \cdot (1 - frsn) && \text{(bare soil)} \\
& + E_{SN} \cdot frsn && \text{(snow cover)}
\end{aligned} \qquad (3)
$$

where

frfor = fraction forest; *fropl* = fraction open land; *frsn* = fraction snow cover
$E_{TR\delta}$ = total transpiration rate with regard to canopy water (Eqs. (4) and (28))
E_R = evaporation of liquid water intercepted on the canopy
E_G = evaporation from bare soil part not covered by vegetation elements
E_{SN} = evaporation from snow cover.

The vegetation canopy evapotranspiration $(E_R + E_{TR\delta})$ is multiplied with *frfor+fropl (=1)* when there is no snow *(frsn=0).* With complete snow cover *(frsn=1),* canopy evaporation takes part only from the forest canopy assuming that the snow is on the

forest floor. In that case, there is no canopy evaporation from open land since the snow covers the vegetation canopy. *frsn* is calculated with the hydrological snow model described below. In the evapotranspiration components described below, *veg* is the area fraction covered by vegetation parts. $q_{sat}(T_s)$ is the atmospheric saturation specific humidity (kg kg^{-1}) at surface temperature T_s. q_a is the specific humidity at the lowest model level (at about 30 m).

3.1 Transpiration from dry vegetation

The total transpiration is the sum over the two soil layers used for soil moisture, of thicknesses D_{w1}=0.072 m (top layer) and D_{w2}=0.8 m (deep layer):

$$E_{TR} = E_{TRd} + E_{TRs} \tag{4}$$

E_{TRd} and E_{TRs} are the transpiration rates for the dry vegetation canopy transporting moisture from the deep soil layer and top soil layer respectively,

$$E_{TRd} = \frac{\rho \cdot veg \cdot \Delta q}{r_{sd} + r_a} \frac{D_{w2}}{D_{w1} + D_{w2}} \tag{5}$$

$$E_{TRs} = \frac{\rho \cdot veg \cdot \Delta q}{r_{ss} + r_a} \frac{D_{w1}}{D_{w1} + D_{w2}} \tag{6}$$

Δq is the saturation deficit between the surface and the lowest model level:

$$\Delta q = q_{sat}(T_s) - q_a \quad (\text{kg kg}^{-1}) \tag{7}$$

veg describes a property of the vegetation cover, namely the area fraction covered by vegetation elements. The remainder (1- *veg*) corresponds to the bare soil fraction. For *veg*, the value 0.9 is used for open land and 0.99 for forest. *veg* is weighted according to

$$veg = 0.9 \cdot fropl + 0.99 \cdot frfor \tag{8}$$

The surface resistances for the two soil layers differ only with respect to their soil properties, that is by differing f_{2d} and f_{2s}:

$$r_{sd} = \frac{r_{s\,\min}}{LAI} \frac{f_1}{f_{2d} \cdot f_3 \cdot f_4} \tag{9}$$

$$r_{ss} = \frac{r_{s\,\min}}{LAI} \frac{f_1}{f_{2s} \cdot f_3 \cdot f_4} \tag{10}$$

f_{2d} and f_{2s} give effects of soil water stress in the deep soil layer and top soil layer, respectively. These parameters and transpiration are reduced when soil moisture in either layer is below 90% of field capacity. The formulation implies the same root density in both layers. Transpiration is also reduced when there is frozen water in either layer. Thus, for deep layer soil temperature, T_d, below +1 °C, f_{2d} is reduced due to reduced liquid soil water available for transpiration by f_{LIQd}, the fraction of unfrozen soil water in this layer. For T_d < -3 °C only frozen soil water exists and f_{LIQd} = 0. For T_d > +1°C only liquid soil water exists and f_{LIQd} = 1. Between these temperatures, f_{LIQd} is

obtained by a sinusoidal interpolation. For f_{2s} there is a corresponding relation depending on f_{LIQs} calculated in the same way from the top layer soil temperature T_s. The expressions for the dependence of f_{2d} and f_{2s} respectively, on soil moisture and on frozen soil become,

$$f_{2d} = \min\left(1.0, \frac{w_d}{w_{FC\,d}} \cdot \frac{f_{LIQd}}{0.9}\right) \tag{11}$$

$$f_{2s} = \min\left(1.0, \frac{w_s}{w_{FC\,s}} \cdot \frac{f_{LIQs}}{0.9}\right) \tag{12}$$

E_{TRd} and E_{TRs} transport moisture from the deep soil layer and top soil layer respectively. When a soil layer becomes very dry, the transpiration rate is suppressed by an exponential soil moisture decay with a time constant (time for reduction by the factor 1/e) of the order of one month if Δq is of the order of 0.01 kg kg^{-1}. In the code, this is achieved by multiplying, in the expressions for E_{TRd} and E_{TRs}, both the numerator and the denominator by f_{2d} and f_{2s} respectively. This avoids calculating surface resistance dividing by f_{2d} and f_{2s} when they are very small, as for very dry soils, and is necessary in order to prevent transpiration from exceeding the available soil moisture.

The calculation of f_1, f_3 and f_4 follows the ISBA (Interaction Soil-Biosphere-Atmosphere) model described by Noilhan and Planton (1989). f_1 reduces r_s with increasing daylight by

$$f_1 = \frac{1+f}{f + r_{s\min}/5000} \qquad f = 0.55\frac{R_g}{R_{sa}}\frac{2}{LAI} \tag{13}$$

where R_g is global radiation in Wm^{-2} and R_{sa} is a limit value for R_g,

$$R_{sa} = fropl \cdot 100 + frfor \cdot 30 \tag{14}$$

LAI occurring in f_1 (and in the rainfall interception model) is weighted as

$$LAI = fropl \cdot laiopl + frfor \cdot laifor \tag{15}$$

The values of *laiopl* and *laifor* are interpolated for different kinds of vegetation as described below.

f_3 increases r_s when the air vapour pressure deficit is high. It includes an empirical parameter α interpolated between 0 for open land and 40 for forest,

$$f_3 = 1 - \alpha\,(q_{sat}(T_a) - q_a) \tag{16}$$

$$\alpha = fropl \cdot 0 + frfor \cdot 40 \tag{17}$$

f_4 describes the influence of air temperature by

$$f_4 = \max\left[10^{-6}, 1 - \left(\frac{25 - T_a}{25}\right)^2\right] \tag{18}$$

r_s is made smallest at T_a = 25°C when f_4=*1* and very large for $T_a \leq$ 0°C or $T_a \geq$ 50°C when $f_4 = 10^{-6}$. T_a is air temperature at the lowest model level expressed here in °C.

r_{smin} (sm^{-1}) is a base value of surface resistance weighted as

$$r_{s\min} = \left(\frac{fropl}{100} + \frac{frfor}{250} \right)^{-1} \tag{19}$$

For use in the factor f_1, the values 100 and 250 sm^{-1} of surface resistance are used for open land vegetation and forest, respectively.

In the expressions for surface resistance above, r_{smin}/LAI occurs as a ratio. The inverted value of this ratio is obtained by weighting the ratio as a whole:

$$\left(\frac{LAI}{r_{s\min}} \right)_{weighted} = \frac{fropl \cdot laiopl}{100} + \frac{frfor \cdot laifor}{250} \tag{20}$$

The inverted values of both r_{smin} and r_{smin}/LAI are weighted here, because they are more closely related to the evapotranspiration fluxes and are therefore considered to give a more proper weighting. The components *laiopl* and *laifor* of leaf area index *LAI* are described below. In general, the parameter values for open land and forest used above derive mainly from the ISBA model but for r_{smin}, *LAI* and *veg* some information from studies in the NOPEX area in Sweden (Bringfelt et al. 1999) has been added.

3.2 Rainfall interception

In summer the evaporation of rainfall intercepted on a forest can amount to the order of 25% or more of total rainfall. If the rain falls as showers, most of the intercepted water will evaporate during the time intervals between them, and the interception loss will be a larger part, than if rainfall is distributed more uniformly in time. In RCA2 a rainfall interception model similar to ISBA is used for low and high vegetation canopies as shown in Fig. 1. Interception is used also for a forest canopy with snow cover on the forest floor. The water stored on the canopy has been adopted as a separate forecast variable, w_r. The canopy water amount at the end of a time step, w_r^+, is calculated from the initial water amount, w_r, the rainfall amount RA_F and the evaporation rate E_R. Δt is the time step length used.

$$\frac{w_r^+ - w_r}{\Delta t} = veg \cdot RA_F - E_R \tag{21}$$

If w_r^+, calculated for the time step, exceeds the water capacity w_{rmax} of the canopy,

$$w_{r\max} = 0.2 \cdot LAI \cdot veg \quad (\text{kg m}^{-2}) \tag{22}$$

the surplus of water will fall to the ground as throughfall. It will contribute in place of rainfall to the soil water budget.

The evaporation part is the product of maximum possible evaporation of water from the canopy and the relative water coverage δ:

$$E_R = \rho \cdot veg \cdot \frac{\Delta q}{r_a} \cdot \delta \tag{23}$$

$$\delta = \left(\frac{w_r}{w_{r\max}} \right)^{2/3} \tag{24}$$

In RCA2 an implicit solution is used to achieve better numerical performance, so that δ is averaged between the initial and final water amounts for the time step:

$$\delta = 0.5 \cdot \left[\left(\frac{w_r}{w_{r\max}} \right)^{2/3} + \left(\frac{w_r^{+}}{w_{r\max}} \right)^{2/3} \right] \tag{25}$$

w_r^+ is solved implicitely by the Newton-Raphson method, described in elementary text books.

3.3 Treatment of wet vegetation

Morén et al. (2000) briefly discuss transpiration from water saturated vegetation where the ISBA model gives no transpiration. This is modelled here by letting the canopy water exist as droplets. A droplet has a curved water surface and covers a smaller plane leaf surface. The exponent *2/3* in the expression given above for δ, the surface of the water droplets, is simply obtained assuming the droplets being half spheres or whole spheres (for the extreme case of the droplets just touching the leaf surface). This is the case because the water volume w_r is proportional to Nr^3 and the water surface of the droplets (δ) is proportional to Nr^2, where N is the number of droplets and r is their radius. Interception evaporation is proportional to the water surface δ. Since the water storage w_r is proportional to Nr^3, δ becomes proportional to $w_r^{2/3}$ as given above. Transpiration is proportional to $(1 - k\delta)$ where $k\delta$ simulates the plane vegetation surface "shaded" by the droplets. k is a measure of the part of the water droplets covering the vegetation surface.

k=0: Droplets are full spheres just touching the vegetation surface (transpiration from the whole leaf surface).

k=1: If the canopy is wet, *(δ=1)*, a water film covers the vegetation completely and there is no transpiration (corresponds to the previous ISBA model).

Letting $k < 1$ will allow for transpiration from a completely saturated canopy where $\delta=1$. In order to adhere to the model discussed above, where the canopy water exists as droplets, a rather small value of k was used: *k=0.25*. The Halstead coefficient h_v, a factor in the total evapotranspiration flux from the vegetation canopy becomes:

$$h_v = \underbrace{1 - si(1-\delta)}_{\text{canopy water evaporation/ condensation}} + \underbrace{si(1-k\delta)\frac{r_a}{r_s + r_a}}_{\text{transpiration}} \tag{26}$$

If the vertical humidity gradient shows condensation *(Δq<0), si=0* otherwise *si=1*. The complete fluxes used in the presence of canopy water are:

$$E_R = \rho \cdot veg \cdot \frac{\Delta q}{r_a} \cdot [1 - si(1-\delta)] \tag{27}$$

$$E_{TR\,\delta} = E_{TR} \cdot si(1 - k\delta) \tag{28}$$

E_{TR} is the transpiration from a completely dry canopy as calculated in Equations (4), (5) and (6). According to the ISBA model, the above treatment means that condensation takes place on the whole canopy but evaporation (transpiration) takes place from the water covered (water free) part. In contrast to ISBA, k<1 implies that transpiration takes place also from a completely wet canopy. The change only consists of introducing the factor k above. This implies no change in the evaporation of intercepted water as formulated for a time step. The overall total transpiration will be somewhat larger since transpiration from a wet canopy is now allowed.

3.4 Bare soil evaporation

This is the evaporation from the area fraction not covered by vegetation elements i.e. the bare soil:

$$E_G = \rho \frac{(1-veg)\Delta q}{r_{soil} + r_a} \tag{29}$$

$$r_{soil} = 50 / ff \qquad \text{where} \qquad ff = f_{LIQs} \cdot w_s / w_{FCs} \tag{30}$$

As above, f_{LIQs} is the fraction of liquid (non-frozen) soil water to total soil water in the top soil layer. When the top soil layer moisture is at field capacity (w_s=w_{FCs}) and the soil is not frozen, r_{soil} = 50 s m^{-1} (van den Hurk et al. 2000). r_{soil} is increased (because $ff < 1$) when w_s<w_{FCs} or if frozen water exists. Thus, r_{soil} is increased by frozen soil as described for transpiration above but now the top soil layer temperature T_s is used. E_G transports moisture from the top soil layer. When the top soil layer becomes very dry, r_{soil} will suppress the evaporation rate by an exponential soil moisture decay with a time constant (time for reduction by the factor e^{-1}) of about a month or less if Δq is of the order of 0.01 kg kg^{-1}.

3.5 Snow evaporation

For forest, it is assumed that all the snow lies on the ground, that is, no snow interception model for the forest canopy is used. The following expression is used:

$$E_{SN} = \rho \cdot \Delta q \cdot [\frac{fropl}{r_{aopsn}} + \frac{frfor}{\max(\ 16\ r_{afosn}\ ,400\ )}] \tag{31}$$

For snow cover on open land the roughness length value of 0.001 m is used in calculating r_{aopsn}, the value of aerodynamic resistance as outlined above. For getting the forest aerodynamic resistance, r_{afosn}, the roughness value of 1.0 m is used. The factor 16 accounts for the increased resistance of the canopy air compared to the aerodynamic

resistance and was estimated from a model presented by J. Shuttleworth in Schmugge and André (1991). The value 400 is used to ensure a large value of canopy air resistance even in unstable or windy conditions (small r_{afosn}). In Equation (31), the evaporation fluxes are weighted according to the area fractions of these two land cover types.

In calculating Δq in (31), 0˚C is used instead of T_s when $T_s > 0$˚C; that is, $\Delta q = q_{sat}[min (0˚, T_s)] - q_a$. The purpose is to reduce snow evaporation when the surface temperature is above 0˚C, but to retain the value of T_s for calculating the sensible heat flux.

4 Weighting of the leaf area index

As described above, the leaf area index affects transpiration and rainfall interception. It is interpolated for the day of calculation from the values in Table 1 that are valid for the middle of each month. The same values are used even in climate change simulations, that is, eventual effects of changing climate on the leaf area index are neglected.

Table 1. *Mid-month values of leaf area index used for open land, deciduous forest and coniferous forest.*

	J	F	M	A	M	J	J	A	S	O	N	D
Laiopl	0.4	0.4	0.4	0.4	0.64	1.28	1.6	1.6	1.28	0.64	0.4	0.4
Laidec	0.4	0.4	0.4	0.8	1.6	3.2	4	4	3.2	1.6	0.8	0.4
Laicon	3.25	3.25	3.25	3.33	3.5	3.83	4	4	3.83	3.5	3.33	3.25

The monthly values of *laidec* are used for deciduous forest (with no leaves in winter). The non-zero values of *laidec* in winter simulate the bare trees with some capacity for rainfall interception. For coniferous forest, Prof. Anders Lindroth (Lund University) gives four years as the typical life time of a pine needle and ten years for a spruce needle. For a mixed coniferous forest the winter LAI is estimated to be half-way between 75% and 90% of the summer LAI, i.e. 82.5% of this. Since the summer LAI is 4, then winter LAI becomes 3.25. For other seasons, interpolation is made similarly as for other vegetation types. The winter coniferous LAI is unimportant for transpiration due to restrictions of surface resistance (Section 3.1) so the main influence is for rainfall interception. The total forest leaf area index, *laifor* is obtained as,

$$laifor = laidec \cdot decid + laicon \cdot (1 - decid) \tag{32}$$

where *decid* is the fraction of deciduous forest to total forest. *laiopl* and *laifor* are the values used in the calculation of total *LAI* described above.

The fraction of the total forest area that is deciduous, *decid*, is assigned to different parts of Europe according to Table 2.

Table 2. *Values, used in the model, for the fraction of deciduous forest to total forest (decid) deduced for different parts of Europe.*

Latitude	Longitude	*decid*	
> 60ºN		15%	(northern Scandinavia, Finland, northern Russia)
52-60ºN	< 25ºE	25%	(southern Scandinavia, northern central Europe)
52-60ºN	> 25ºE	40%	(middle Russia)
< 52ºN	< 0ºE	30%	(Iberian Peninsula, western France)
< 52ºN	> 0ºE	40%	(other parts of central and southern Europe)

The values of *decid* were obtained as follows: From 1º × 1º fields of Henderson-Sellers (HS) class in Europe (Arpege-Climat 1996), a forest class was assigned from the primary HS class or, if this is not a forest class, from the secondary HS class. For the forest HS classes standard deciduous percentages were assigned according to Table 3.

Table 3. *Standard percentages of deciduous forest used to derive the values in Table 2.*

HS class	Forest type	Deciduous forest
3	Evergreen needle tree	0%
5	Deciduous broadleaf tree	100%
6	Evergreen broadleaf tree	0%
18	Mixed woodland	50%

The percentage fraction of deciduous forest in a grid square was calculated from the HS class in the grid itself and in the eight surrounding grids. This area averaging was needed because the HS classes may change drastically from grid to grid and some grids have no forest class.

5 Surface hydrological processes

The new parameterizations for the surface hydrological processes in RCA2 are based on the formulations of the original HIRLAM surface scheme using modified expressions for hydraulic diffusivity, complemented with hydrological processes from the HBV model. The land-surface part of the hydrological cycle, as parameterized in RCA2, is shown in Fig. 1. The time tendency is solved for soil moisture in two layers, a shallow (D_{w1}=0.072 m) top layer for w_s and a deep layer (D_{w2}=0.8 m) for w_d, and for the snow depth *SN*. Unlike soil temperature, no relaxation is made to external values.

Equations are solved for soil moisture in the top layer (w_s) and the deep layer (w_d), as below,

$$\frac{\partial w_s}{\partial t} = \frac{\lambda(w_d - w_s)}{0.5 D_{w1}(D_{w1} + D_{w2})} - (1 - frsn)E_G - [frfor + fropl(1 - frsn)]E_{TRs\delta} + RA_{THR} + SN_M - Q_1 \tag{33}$$

$$\frac{\partial w_d}{\partial t} = -\frac{\lambda(w_d - w_s)}{0.5 D_{w2}(D_{w1} + D_{w2})} - [frfor + fropl(1 - frsn)]E_{TRd\delta} + Q_1 - Q_2 \qquad (34)$$

Not shown in these equations is that if at the end of a time step top layer soil moisture exceeds the field capacity value w_{FCs}, there is an additional drainage down to the deeper layer. Correspondingly, if the deeper layer soil moisture exceeds w_{FCd}, there will be an extra contribution to runoff. The parameters used here are summarized in Table 4.

Table 4. *Parameters used for snow and soil processes. Units are indicated only if different from the preceding parameter.*

SN	= snow depth (kg m^{-2} = mm of water)
SN_F	= snowfall rate (kg m^{-2} s^{-1})
RA_F	= rainfall rate
RA_{THR}	= throughfall rate
SN_M	= snowmelt rate
$E_{TRs\delta}$	= transpiration rate from the vegetation canopy draining the top soil layer, corrected for canopy water δ
$E_{TRd\delta}$	= transpiration rate from the vegetation canopy draining the deep soil layer, corrected for canopy water δ
E_{TR}	= E_{TRs} + E_{TRd} = total transpiration rate from the dry vegetation canopy
E_R	= rate of evaporation of liquid water intercepted on the canopy
E_{SN}	= rate of evaporation from snow cover
E_G	= evaporation from bare soil part
Q_1	= drainage rate from the 1st (top) to the 2nd (deep) soil layer
Q_2	= runoff (from 2nd soil layer)
w_s	= top soil layer soil moisture (kg m^{-2})
w_d	= deep soil layer soil moisture
w_r	= canopy water
veg	= fraction of surface covered by vegetation parts
λ	= hydraulic diffusivity (m^2 s^{-1}) due to capillary forces; depends on soil type and soil moisture

The maximum amount of soil water, the field capacity value w_{FCs}, corresponds to 20 mm of water in the top soil layer. The deep layer field capacity w_{FCd} is scaled according to the thickness ratio between the deep layer and the top layer: 20 · 0.8 / 0.072 = 222 mm. The total soil water amount corresponding to field capacity is thus 20 + 222 = 242 mm.

5.1 Hydrological soil moisture and runoff model

In addition to the transport of soil moisture by diffusive (capillary) forces, to be discussed below, runoff generation is here routed down the soil column as in the hydrological HBV model (Bergström 1976, 1995; Lindström et al. 1997), instead of discarding excess water as surface runoff generation. The HBV model equations give

the fraction of rainfall plus snowmelt, used for drainage flow to the second soil layer (Q_1) and for final runoff from this layer (Q_2), as shown in Fig. 1.

$$Q_1 = (RA_{THR} + SN_M) \cdot \left(\frac{w_s}{w_{FC\,s}} \right)^{\beta_1} \qquad Q_2 = Q_1 \cdot \left(\frac{w_d}{w_{FC\,d}} \right)^{\beta_2} \tag{35}$$

The exponents β_1 and β_2 reflect areal variability of soil moisture. Because of this variability, runoff can occur even if the area averages w_s and w_d are below their corresponding field capacity values w_{FCs} and w_{FCd}. β_1 and β_2 are both given the value 2, a typical value used in HBV model applications where β can range from 1 to 4 (Bergström 1990). The equations have a stabilizing effect on soil moisture because runoff is large (small) when soil moisture is large (small).

5.2 Hydraulic diffusivity

The hydraulic diffusivity λ described below and used in Equations (33) and (34) (based on Clapp and Hornberger 1978 and McCumber and Pielke 1981) gives the rate of vertical exchange of soil moisture due to capillary forces. It is calculated using 1) the geographical distribution of soil types (FAO-Unesco 1981) digitized for Europe by the German Weather Service and 2) the value of soil moisture. Table 5 lists the parameter values used for calculating λ for different soil types.

Table 5. *Parameter values for the soil types used. Type 6 stands for equal parts of sand and clay and is treated as loam.*

Soil texture class		1 Sand	2 Loam	3 Clay	4 Sandy Loam	5 Silt Loam	6 Sandy Clay (Loam)	7 Peat
Volumetric soil moisture limits in m^3m^{-3}								
θ_{sat}	Saturation	0.395	0.451	0.482	0.435	0.485	0.451	0.863
θ_{fc}	Field capacity	0.135	0.240	0.367	0.195	0.255	0.240	0.480
θ_{wi}	Wilting point	0.068	0.155	0.286	0.114	0.179	0.155	0.395
Ψ_{sat} saturation moisture potential in m								
$100\psi_{sat}$		12.1	47.8	40.5	21.8	78.6	47.8	35.6
Clapp and Hornberger exponent b								
		4.05	5.39	11.4	4.90	5.30	5.39	7.75
Saturation hydraulic conductivity γ_{sat} ($m\ s^{-1}$)								
$10^6\gamma_{sat}$		176	6.95	1.28	34.7	7.20	6.95	8.0
Volumetric heat capacity for dry soil, $(c \cdot \rho)_{dry}$ ($Jm^{-3}K^{-1}$)								
		1280	1350	1420	1350	1350	1350	580

The volumetric soil moisture θ (m^3m^{-3}) is calculated from the deep layer soil moisture w_d ($kg\ m^{-2}$) by,

$$\theta = \frac{w_d}{w_{FCd}}(\theta_{fc} - \theta_{wi}) + \theta_{wi} \tag{36}$$

The hydraulic diffusivity for soil moisture (m^2s^{-1}) is written as,

$$\lambda = -\frac{b\gamma_{sat}\psi_{sat}}{\theta}\left(\frac{\theta}{\theta_{sat}}\right)^{b+3} \tag{37}$$

Hydraulic and thermal parameters described here and in Section 7 are calculated using θ/θ_{sat}, i.e. scaling is made to saturated volumetric soil moisture (which corresponds to the total porosity of the soil), whereas the maximum possible volumetric soil moisture is at field capacity. The geographical distribution of soil texture classes and calculated hydraulic diffusivity are shown by Rummukainen et al. (1998; Figs. 9-10).

The terms in Equations (33) and (34) for the vertical transport of soil moisture, use the hydraulic diffusivity λ. These terms, used also in the original surface scheme for HIRLAM, describe capillary and adhesive forces which can lift or lower moisture from a moist soil layer to a drier layer as discussed by Rummukainen (1999). When there is active vegetation, transpiration flux dominates over the hydraulic transfer. These hydraulic terms are retained here because they are considered realistic when there is no or weak transpiration as in autumn and spring. Using only the HBV model equations without the hydraulic terms, the top soil layer will remain wet after a rainfall if no evaporation or transpiration takes place from the soil. Then the choice of soil layers (their number and thicknesses) will strongly influence the vertical moisture profile. Using the hydraulic terms will even out the profile in time, making the choice of soil layers less critical.

6 Hydrological snow model

A snow model has been introduced in RCA2 that includes a statistical subgrid treatment of the fractional area of snow cover and snow melt rate using the variance of topography height (Lindström and Gardelin 1999) based on experience with the HBV hydrological model (Bergström 1976; Lindström et al. 1997). The snow covered area fraction *(frsn)* is larger when the snow pack is building up than in snowmelt episodes when the snowpack is reduced into patches. This is achieved using the previously reached maximum snow depth, SN_{max} (see Fig. 2), as a forecast variable in addition to the snow amount *SN*. In Section 13 an example of the behaviour of these variables is discussed.

The original HIRLAM formulation gives *SN*, the total snow amount in mm (or kg m^{-2}) of water evolving as

$$\frac{\partial SN}{\partial t} = SN_F - SN_M - frsn \cdot E_{SN} \tag{38}$$

To get the snowfall rate, SN_F, the time step value *dsnowdt* (mm s^{-1}) available directly from the HIRLAM precipitation scheme is used:

$$SN_F = dsnowdt \tag{39}$$

According to the hydrological formulation of Lindström and Gardelin (1999), snow falls over the area fraction *(1-amelt)*, the fraction of grid area with temperature below 0ºC. As an alternative the value

$$SN_F = (1\text{-}amelt)\ (draindt + dsnowdt) \tag{40}$$

could be used, but this would be less consistent with other parts of the HIRLAM physics.

6.1 Snowmelt

The following degree-day equation from hydrological modelling is used for the snowmelt rate,

$$SN_M = cfmax \cdot Temp^{+} \cdot frsn \cdot amelt \qquad \text{(mm/24 hours)} \tag{41}$$

Open land: $cfmax$ = 3.5 mm/(^{o}C · 24 hours)
Forest: $cfmax$ = 2.0

The notations will be explained below. The values of *cfmax* are based on the HBV hydrological model (Bergström 1990). SN_M becomes proportional to the snow-covered area with above-zero temperature (described below): *frsn* · *amelt*. Snowmelt may then occur even if the mean grid temperature is below 0ºC. Together with rainfall, snowmelt acts to increase soil moisture.

A snow melt term, M_{eff}, is subtracted from the energy balance for the surface temperature tendency (discussed in Section 7),

$$M_{eff} = SN_M \cdot L_f / (24 \cdot 3600) \tag{42}$$

where L_f is the latent heat of fusion (J/kg). *amelt,* the fraction of grid area with temperature above 0ºC, is

$$amelt = \min\left[\frac{\max(T\max,0)}{TTI},\ 1\right] \qquad \text{(Temperatures in ºC)} \tag{43}$$

With a temperature lapse rate of 0.6 ºC per 100 m, commonly used in the HBV model, a temperature interval (TTI) was assumed over the grid square as a function of the elevation range *(Hmax-Hmin),* see Fig. 2. *TTI = 2 + 0.6(Hmax-Hmin),* where *Hmax-Hmin = √12 · orosigm.* The minimum value of *TTI* (2ºC) accounts for temperature variations between different parts of an area even without elevation differences. *orosigm* is the standard deviation of orography obtained from the GTOPO30 database (Section 10.2).

Since,

$$Tmin = Tmean - TTI/2$$

$$Tmax = Tmean + TTI/2 \qquad (44)$$
$$Tmean = (Tmax + Tmin)/2$$

the temperature $Temp^+$ over the surface fraction *amelt* is,

$$Temp^+ = Tmean \qquad \text{if} \quad Tmin > 0ºC \qquad (45)$$

$$Temp^+ = Tmax/2 \qquad \text{if} \quad Tmin \le 0ºC \qquad (46)$$

Tmean is the grid box average temperature. For hydrological modelling applications calibration is carried out using observed screen level temperature. In HIRLAM this corresponds to the temperature at 2m height (*T2m*) interpolated between the temperatures at the surface and at the lowest atmospheric model level. As alternatives for calculating *Tmean*, we then have the HIRLAM variables *T2m* (which is diagnostic and represents the whole grid square including its open water fraction) and also the land plus ice surface temperature T_s, which is used in the present RCA2 version.

In hydrological modelling, *Tmean* is a 24 hr mean value, but in HIRLAM a timestep length from 5 to 20 min is used. To investigate the use of shorter time averages than 24 hours, *cfmax* was derived from the HBV model using daytime and nighttime 12-hourly values, giving only minor differences in *cfmax* compared to using 24-hr values. Therefore, no correction has been made for using the shorter HIRLAM timestep.

The area fraction of snowcover *frsn* is calculated from the present and previous maximum snow amounts:

$$frsn = \frac{SN}{SN_{\max} \cdot sfdist} \quad if \;\; SN / SN_{\max} \le sfdist \qquad (47)$$

$$frsn = 1 \qquad if \;\; SN / SN_{\max} > sfdist \qquad (48)$$

For simplicity, *sfdist = 0.6* is used everywhere. As pointed out by Lindström and Gardelin (1999), *1-sfdist* determines the amount of snow that has to melt before any bare ground appears.

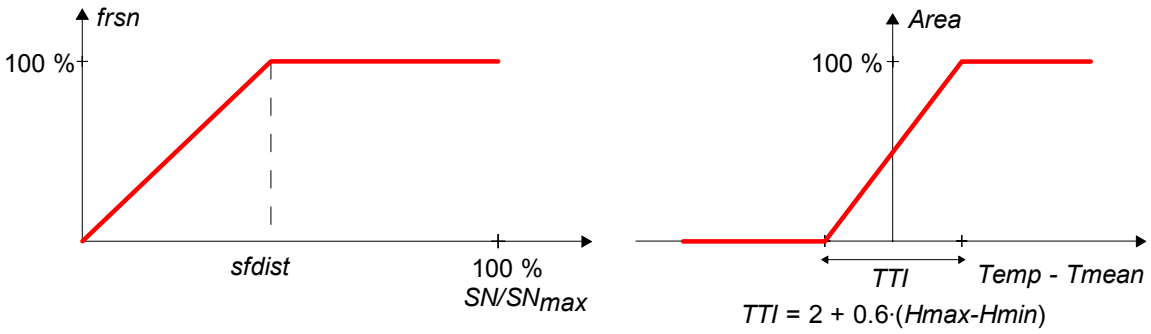

Figure 2. *Left: modelled snowcover as a function of snow amount. Right: modelled temperature distribution over an area.*

6.2 Calculation of new timestep value of maximum snow depth

The maximum snow depth, SN_{max}, is the latest previous maximum value of snow amount, SN. If the new value of snow depth SN^+ exceeds SN_{max}, then SN_{max}^+ will increase to SN^+. Like the variable SN, SN_{max} has to be stored for the next HIRLAM timestep.

The following algorithm, a development for HIRLAM as compared to the hydrological model of Lindström and Gardelin (1999), will automatically let SN_{max} decrease to zero during a long snowfree period, such as a summer season. If SN^+ is smaller than $k_1 \cdot SN_{max}$, k_1=0.2 and $k = exp(-10^{-6} \cdot 2\Delta t)$ where Δt is the length in seconds of the HIRLAM timestep,

$$SN_{\max}^{+} = SN_{\max} - (k_1 \cdot SN_{\max} - SN) \cdot (1 - k) / k_1 \tag{49}$$

This is used when SN has fallen below a treshold value (20%) of SN_{max}. Then SN_{max} will be reduced in each time step by a factor dependent on k and the deficiency of SN below $k_1 \cdot SN_{max}$. If $SN=0$ we get $SN_{max}^+ = k\ SN_{max}$, and if the expression for k given above is used, SN_{max} will decrease to 1% of its original value in about 26 days. If SN^+ is between $k_1 \cdot SN_{max}$ and SN_{max}, no substantial snow decline is considered to occur, and SN_{max} will not change.

6.3 Snow density

Snow density affects forecast surface temperature because dense snow has greater volumetric heat capacity and diffusivity. In a snow model of Douville et al. (1995) snow density values between 100 and 300 kg m^{-3} are used. In earlier versions of RCA, a set of monthly snow density values ρ_{month} from measurements were used (Eerola 1996). The values from January to December are (kg m^{-3}): 220, 230, 240, 280, 320, 320, 320, 320, 100, 160, 180, 210. The smallest density, 100 kg m^{-3}, was used for September. The values increase during the winter, due largely to settling of the snow pack. These values are still used but are modified depending on the ratio between SN and SN_{max} which are both prognostic variables. In a snow melt period SN/SN_{max} becomes reduced and the reduced value is retained when the temperature falls below freezing. The following expression is used for snow density ρ_{sn} (kg m^{-3}):

$$\rho_{sn} = \rho_{month} + 198 - 220 \cdot (SN / SN_{max}) \tag{50}$$

The final value of ρ_{sn} is kept limited between 100 and 320 kg m^{-3}. With snow depth SN near SN_{max}, no or a small change is made to the monthly standard value. With SN/SN_{max} near zero most snow has melted and a maximum increase (198 kg m^{-3}) in snow density is possible. The magnitude of the snow density interval given above, is 220 kg m^{-3}. In Equation (50), the correction to ρ_{month} is between –22 and 198 kg m^{-3} instead of 0 to 220 kg m^{-3}, to account for the possibility of somewhat enhanced snow density values of Eerola due to snow melt periods in his data. The method makes regard to areas which may often have more snow melt periods than southern Finland, where the original data were measured. The method was introduced to reduce low forecast snow temperatures

in winter. In a three-dimensional test, the change gave slightly increased winter temperatures, but the effect was relatively small.

7 Equations for the soil temperature

The temperature layers of the soil are the same as in the original HIRLAM surface scheme with a top layer of depth D_1=0.072 m, a second layer of depth D_2=0.432 m and a climatological bottom layer of depth 0.432 m centered at the bottom of the second layer. The equations are,

$$\frac{\partial T_s}{\partial t} = \frac{G}{\rho_i c_i D_1} + \frac{\kappa_i (T_d - T_s)}{0.5 D_1 (D_1 + D_2)} \tag{51}$$

$$\frac{\partial T_d}{\partial t} = -\frac{\kappa_i (T_d - T_s)}{0.5 D_2 (D_1 + D_2)} + \frac{\kappa_{soil} (T_{cli} - T_d)}{D_2 D_3} \tag{52}$$

where the volumetric soil heat capacity $\rho_i c_i$ and heat diffusivity κ_i are interpolated according to the fraction of snow *frsn* using the soil and snow values described below. G is the net downward energy flux at the surface from Eq. (1). The climatological layer temperature T_{cli} is interpolated 6-hourly from the driving GCM or ERA data.

Thermal conductivity ($Wm^{-1}K^{-1}$) is given as (Viterbo 1996):

$$\lambda_{heat} = 3.8(-\psi_{sat})^{-1/\ln(10)} \left(\frac{\theta}{\theta_{sat}} \right)^{b/\ln(10)} \tag{53}$$

Thermal diffusivity (m^2s^{-1}), used in the equations, becomes:

$$\kappa_{soil} = \frac{\lambda_{soil}}{c_{soil} \cdot \rho_{soil}} \tag{54}$$

where *soil* stands for the snow free part. The volumetric heat capacity of the soil ($Jm^{-3}K^{-1}$) is interpolated as:

$$c_{soil} \cdot \rho_{soil} = 1000\ (c\rho)_{dry} + 4.19 \cdot 10^6 \cdot \theta \tag{55}$$

where the density and specific heat of water are 1000 kgm^{-3} and 4190 $Jkg^{-1}K^{-1}$. Values of heat capacity including snow cover are interpolated as,

$$c_i \cdot \rho_i = c_{soil} \cdot \rho_{soil}\ (1 - frsn) \quad + \quad c_{sn} \cdot \rho_{sn} \cdot frsn \tag{56}$$

where ρ_{sn} is given above and the heat capacity ($Jkg^{-1}K^{-1}$) of ice is,

$$c_{sn} = 1000\ (\ 2.115 + 0.00779\ T_s\ ) \tag{57}$$

when T_s is in ºC (Gray and Male 1981).

The weighted thermal diffusivity becomes,

$$\kappa_i = \kappa_{soil}\ (1 - frsn) + \kappa_{sn} \cdot frsn \tag{58}$$

where,

$$\kappa_{sn} = \lambda_{ice}\left(\frac{\rho_{sn}}{\rho_{water}}\right)^{1.88}\frac{1}{c_{sn}\rho_{sn}} \tag{59}$$

and λ_{ice} is the heat conductivity for ice, 2.22 $Wm^{-1}K^{-1}$ (Douville et al. 1995).

As in the original HIRLAM version, the total grid area surface temperature T_s may exceed 0ºC for a partial snow cover. This is realistic because the snow free part of the grid area may exceed 0ºC by several degrees. In reality, surface temperature may exceed 0ºC even when the ground is fully snow-covered, due to warmer trees, houses etc. This is possible even in the model, but in this case there is an asymptotic limit to the rise of surface temperature caused by the consumption of energy for snowmelt. With steady energy flux G (Wm^{-2}) to a fully snow-covered surface, neglecting the heat exchange with the deep soil layer, the asymptotic maximum temperature rise is determined by,

$$\Delta T_{s,\max\lim} = \frac{G \cdot 86400}{cfmax \cdot L_f} \tag{60}$$

where L_f(=3.3·10^5 J kg^{-1}) is the latent heat of fusion. For G = 20 Wm^{-2} and $cfmax$ = 3.5 mm per ºC and 24 hours, the maximum temperature rise becomes $\Delta T_{s,maxlim}$ = 1.5ºC. The time required for reaching 63 % (=1-e^{-1}) of the maximum rise is $c_{sn} \cdot \rho_{sn} \cdot D_1 \cdot \Delta T_{s,maxlim}$ / G seconds (in this example about 38 minutes). For a snow cover, the top layer represented by T_s is located at the top of the snow layer. Therefore, $c_i \cdot \rho_i$ and κ_i represent a full or a partial snow cover as described above.

8 Soil freezing and melting

The soil freezing/melting algorithm, based on Viterbo et al. (1999), does not need any additional forecast soil variable. A soil freezing heat flux is added to the equation of the top soil layer in the snow free part of a grid box and to the equation for the deep soil layer. The scheme acts like an increased heat capacity delaying temperature decreases/increases in cooling/heating periods as long as the soil temperature is between –3ºC and +1ºC.

When the soil freezing heat flux $L_f \cdot \rho_w(\partial\theta/\partial t)_d$ (Wm^{-3}) is put into the equation for the second (deep) soil layer temperature T_d, this becomes:

$$(\rho C)_d \frac{\partial T_d}{\partial t} = L_f \rho_w (\frac{\partial \theta}{\partial t})_d + \frac{\partial}{\partial z}(\lambda_T \frac{\partial T}{\partial z})_d \tag{61}$$

$(\rho C)_d$ is volumetric soil heat capacity ($Jm^{-3}K^{-1}$), T is soil temperature, t is time, z is the vertical coordinate, λ_T is thermal conductivity (W m^{-1} K^{-1}), L_f is the latent heat of fusion (J kg^{-1}) and ρ_w water density.

No water is frozen when $T > 1$°C and all water is frozen when $T < -3$°C. For simplicity the soil is always assumed to be at field capacity for these calculations, which is fully realistic only in areas with high winter soil moisture. The frozen soil water amount θ (dimensionless) is assumed proportional to total soil water amount put constant = θ_{FC} :

$$\theta = \theta_{FC} f(T) \tag{62}$$

$f(T)$ is the fraction of water in the ice phase prescribed by:

$$\begin{array}{lll} T < -3\text{ºC}: & f(T) = 1 & \\ -3\text{ºC} \le T \le 1\text{ºC}: & 1 \ge f(T) \ge 0 & \text{(interpolating by a sine relationship)} \\ T > 1\text{ºC}: & f(T) = 0 & \end{array} \tag{63}$$

$$\frac{\partial \theta}{\partial t} = \theta_{FC} \frac{\partial f}{\partial t} = \theta_{FC} f'(T) \frac{\partial T}{\partial t} \tag{64}$$

Putting $T = T_d$, $\partial T_d/\partial t$ is solved by

$$\frac{\partial T_d}{\partial t} = \left(- \frac{\kappa_i (T_d - T_s)}{0.5 D_2 (D_1 + D_2)} + \frac{\kappa_{soil} (T_{cli} - T_d)}{D_2 D_3} \right) [(\rho C)_d - L_f \rho_w \theta_{FC} f'(T_d)]^{-1} \tag{65}$$

9 Melting and freezing of precipitation reaching the ground

9.1 Melting of snowfall on warm, snowfree ground

Since $(1 - frsn) \cdot amelt$ is the snowfree area with above-zero temperature, the melt rate (mm s^{-1}) of snow falling on the warm snow free part is

$$meltfall = dsnowdt \cdot (1 - frsn) \cdot amelt \tag{66}$$

9.2 Freezing of rainfall on cold ground

The freezing rate of rainfall (mm s^{-1}) on cold ground (snow free or snow covered) becomes

$$freezfall = draindt \cdot (1 - amelt) \tag{67}$$

For these two effects the following term (W m^{-2}) will appear in the energy balance:

$$P_{eff} = meltfall \cdot L_f - freezfall \cdot L_f \tag{68}$$

10 Use of basic geographical parameters

10.1 Land-sea mask and forest fraction

For the land-sea mask (*frland*) the standard HIRLAM climate field is used. When RCA is run in stand-alone mode without the lake and Baltic Sea modules, fraction of ice (*frice*) is obtained six-hourly from ERA or GCM data. It is scaled down to the actual

grid resolution used for RCA2. The original forest fraction, $frfor_{MPI}$, is given by the MPI data base (Hagemann 1999). It is based on USGS data available from USGS EROS Data Center. The MPI data is calculated using 1 km fields of 45 ecosystem types allocating climate model parameters to each type. Since the HIRLAM land sea mask and the MPI forest fractions are not totally consistent, the land surface treatment for a grid square with land area computes *frfor* as,

$$frfor = \frac{\min(frland, frfor_{MPI})}{frland} \tag{69}$$

Then, *frfor* is put within the limits 0.01 and 0.99 in order to avoid values which may cause computational problems. Finally *fropl* is calculated as,

$$fropl = 1 - frfor \tag{70}$$

so that the weighting of the vegetation parameters will be made properly. Only vegetated areas are treated in this version of RCA2.

10.2 Topography

The topography used for the hydrological snow model has been converted from GTOPO30, a database available from USGS EROS Data Center. It has a resolution of 30" (0.0083º). The standard deviation of topography needed for the snow model is calculated for the gridsize used in the specific RCA2 simulation.

10.3 Albedo

A temporally constant background albedo field is employed. However, the albedo subroutine only uses this value over land areas where the background albedo exceeds 0.4. This only happens over permanently ice-covered areas such as Greenland. In other areas, standard subsurface albedo values (Bringfelt et al. 1995) are weighted according to the subgrid fractional areas. The albedo is put through a nine-point smoothing to remove strong gradients. The subsurface albedoes are shown in Table 6.

Table 6. *Albedo values used for different kinds of surfaces.*

Surface type	Albedo	
	Value	Name
Water, no ice	0.07	*alwat*
Open land, no snow	0.20	*alopl*
Open land, snow	0.51	*alopsn*
Forest, no snow	0.10	*alfor*
Forest, snow	0.18	*alfosn*
Ice on inland lake (snow or no snow)	0.20	*alice, alicsn*
Ice on sea (snow or no snow)	0.60	*alice, alicsn*

Inland lakes have lower ice albedo than open sea in spring when the albedo is most important (Anders Omstedt, SMHI, pers. comm.). For simplicity, these low spring values are also used in winter, when the albedo is relatively unimportant due to low

incoming shortwave fluxes. The forest snow albedo is kept low (0.18) because it is assumed that the snow lies on the forest floor.

In the albedo routine, the whole grid albedo is obtained by weighting:

$$\begin{aligned} alb = {} & frwat \cdot alwat \\ & + frice \cdot [\, alice \cdot (1\text{-}frsn) + alicsn \cdot frsn \,] \\ & + fropl \cdot [\, alopl \cdot (1\text{-}frsn) + alopsn \cdot frsn \,] \\ & + frfor \cdot [\, alfor \cdot (1\text{-}frsn) + alfosn \cdot frsn \,] \end{aligned} \tag{71}$$

frwat and *frice* are the fractions of open water and ice respectively. *frice* is given regularly by the GCM or ERA boundary fields. *frsn* is calculated according to the hydrological approach described above. *fropl* and *frfor* (their sum here is fraction land) are given by the MPI field for forest fraction. An empirical solar zenith angle correction of the surface albedo is used according to Räisänen et al. (2000).

10.4 Surface roughness

Surface roughness *z0* is used to calculate the surface sensible and latent heat fluxes *H* and *LE* and the momentum flux τ for the grid square. Different *z0*-values for different surface types are used *($z0_{sea}$, $z0_{ice}$* and *$z0_{land}$)* and *H*, *LE* and τ are weighted together to get the grid square fluxes for use in the other HIRLAM physics, primarily the CBR vertical diffusion scheme (Cuxart et al. 2000).

The land roughness $z0_{land}$ is obtained by interpolation, by a method of Mason (1988), between forest and open land using $z0_{for}$ = 1.0 m and $z0_{opl}$ = 0.2 m (*frfor+fropl=1*):

$$\frac{1}{(\ln \frac{l_b}{z0_{land}})^2} = \frac{frfor}{(\ln \frac{l_b}{z0_{for}})^2} + \frac{fropl}{(\ln \frac{l_b}{z0_{opl}})^2} \tag{72}$$

This land roughness is used for calculating *H*, *LE* and τ for land to be weighted together with fluxes for water and ice. No geographical roughness field is used. Only local (related to local surface such as vegetation) roughness is used for both water, ice and land and the fluxes are weighted for each grid square. In earlier vertical diffusion schemes an orographic roughness was also used in order to simulate friction effects from mountain areas. In the CBR scheme this cannot be made since the friction effect is generated from local roughness only.

11 Subgrid weighting of surface fluxes

As discussed above the fluxes of sensible heat, latent heat and momentum are weighted between land, ice and water:

$$H = frwat \cdot H_{wat} + frice \cdot H_{ice} + frland \cdot H_{land} \tag{73}$$

$$E = frwat \cdot E_{wat} + frice \cdot E_{ice} + frland \cdot E_{land} \tag{74}$$

$$\tau = frwat \cdot \tau_{wat} + frice \cdot \tau_{ice} + frland \cdot \tau_{land} \quad (75)$$

12 One-dimensional HIRLAM setup

A one-dimensional version of the HIRLAM physics was used in some of the code development. This enabled quick testing of proposed changes and correction of bugs. The full three-dimensional model gives, for wind, temperature, humidity, cloud water and turbulent kinetic energy at all model levels, dynamical tendencies (from the dynamical part) and physical tendencies (from the physics part). The one-dimensional model may be driven by the three-dimensional model in two ways:

A. By driving the model each timestep with the free atmosphere dynamical tendencies, in the same way as in Gollvik and Olsson (1995)
B. By relaxation of complete free atmosphere profiles from the three-dimensional run.

If we want to study the details of the physics, with feedback mechanisms present, we can omit the relaxation and only rely on the initial state and the prescribed dynamical tendencies (A). This works fine for a shorter period (of the order of two weeks), but due to the chaotic behaviour of the model, this leads eventually to an unrealistic imbalance between the model state and the tendencies. If we want to study the effect on longer time scales like for instance the snow melt process, we must use the relaxation technique (B), completely or partly.

13 Results in selected grid points

During development of the code, numerous three-dimensional fifteen-day runs have been made, where time series plots were studied for one forest-dominated grid point in central Sweden and one open land-dominated grid point in Denmark. The runs were made for different seasons of the year, primarily in order to study diurnal variations of evapotranspiration components and snow processes.

Figs. 3 and 4 show the evapotranspiration components of forest and open land dominated grid points, respectively, for six days in July 1992. Fig. 3 exhibits interception evaporation (E_R) in the morning of 11 July, of canopy water which has rested on the canopy during the night after the rainfall during the preceding day. Bare soil evaporation (E_G) is larger compared to transpiration (E_{TR}) in the open-land dominated point (Fig. 4) than in the forest dominated point (Fig. 3). This is so because a smaller value of *veg* is used for open land.

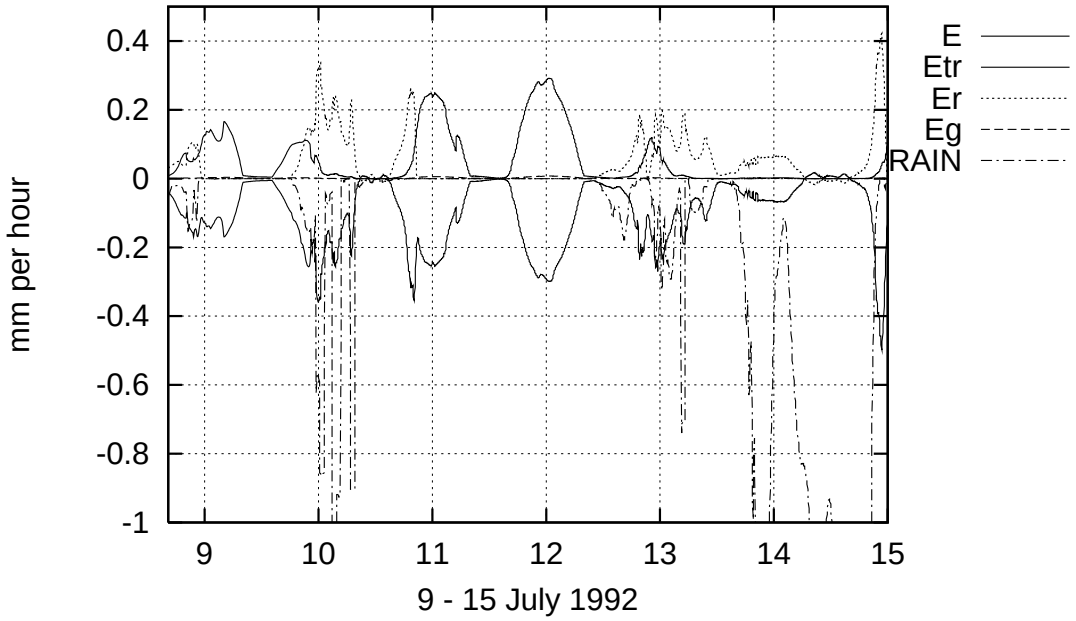

Figure 3. *Evapotranspiration components for a forest-dominated HIRLAM grid point in middle Sweden (61ºN, 14ºE, 93% land of grid area, 99% forest of land area) calculated for six days in July 1992. E – total evapotranspiration sum (counted downwards), E_{TR} – transpiration (counted upwards), E_R – evaporation of water intercepted on the vegetation canopy, E_G – evaporation from the bare soil part. RAIN – rainfall (counted downwards).*

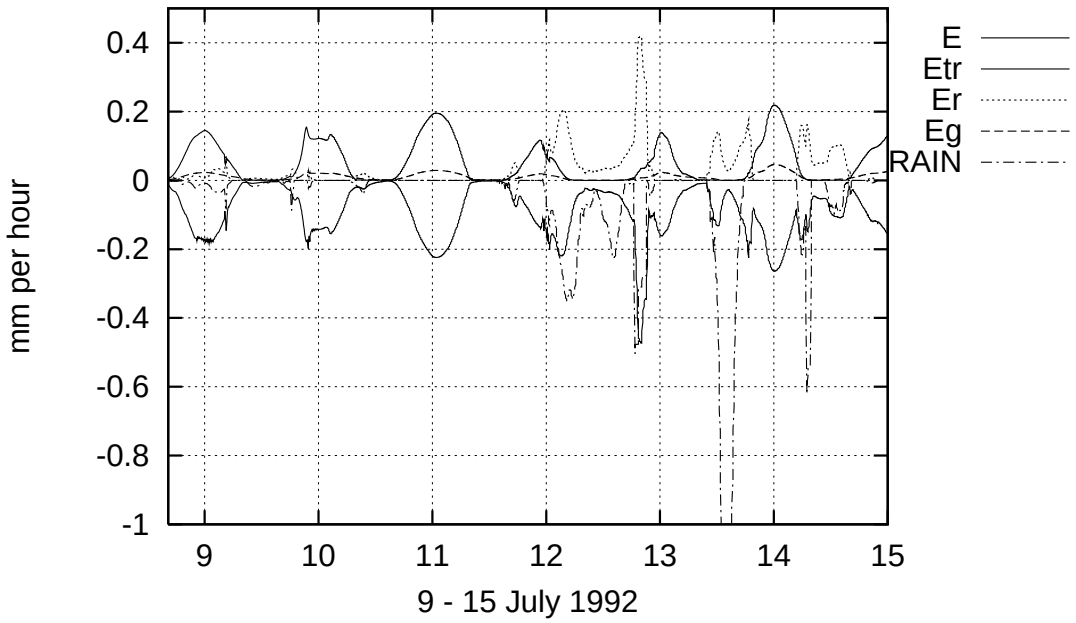

Figure 4. *As Fig. 3, but for an open-land-dominated HIRLAM grid point in western Jutland in Denmark (56.6ºN, 8.5ºE, 55% land of grid area, 94% open land of land area)*

Fig. 5 illustrates the performance of the hydrological snow model. As discussed above the snow covered area fraction (*frsn*) falls below unity when snowdepth *SN* falls below

sfdist·SN_{max}, where *sfdist=0.6.* Also, as described above, the previous maximum snowdepth, SN_{max} is seen to start its decrease when *SN* falls below 20 % of SN_{max}.

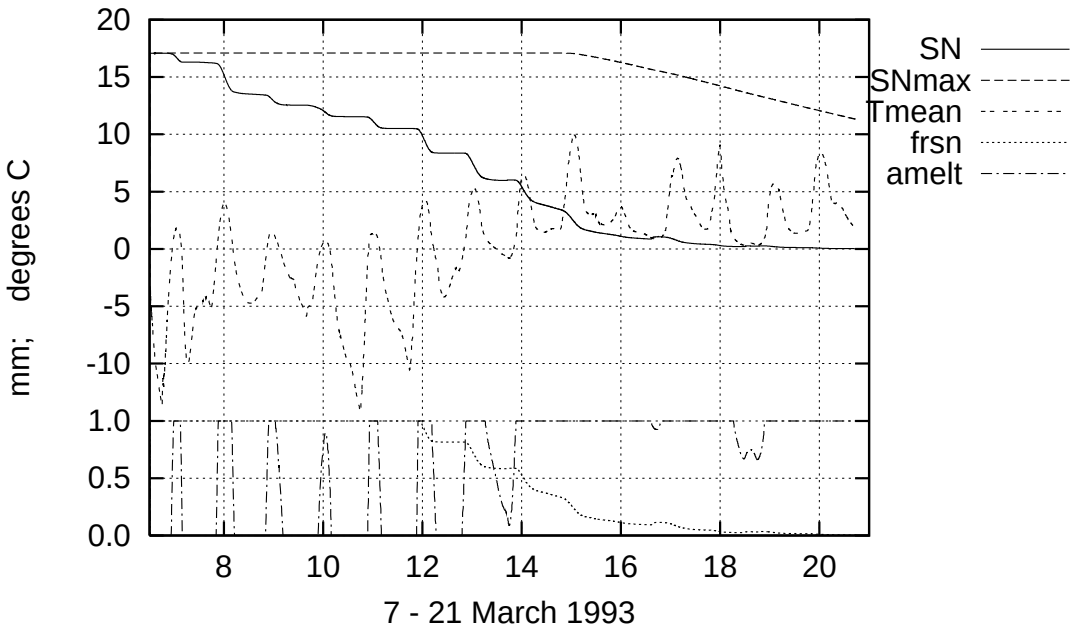

Figure 5. *Snow variables for a forest-dominated HIRLAM grid point in middle Sweden (the same as in Fig. 3) calculated for 14 days in March 1993. SN – snow amount,* SN_{max} *– previous maximum snow amount. Tmean - mean grid area surface temperature. frsn – area fraction of snow cover. amelt – area fraction of temperature above 0ºC.*

14 Results from a five-year three-dimensional model run

The land surface scheme described above was used in a five-year (September 1988 – November 1993) three-dimensional model simulation, driven from boundaries by ECMWF reanalyses (ERA; Gibson et al. 1997). The simulations were made at 44 km resolution, in an area covering 114 × 82 grid boxes in a rotated latitude-longitude grid, and with 24 levels in the vertical. Semi-Lagrangian advection with a 30 min time step was used. The ERA boundary forcing was applied at lateral boundaries and for sea surface temperature (excluding the Baltic Sea) and deep soil temperature. The water temperatures, salinity and ice cover in the Baltic Sea were modelled interactively with the three-dimensional ocean model RCO (Meier et al. 1999). The conditions in inland lakes within the Baltic Sea drainage basin were modelled with the PROBE model (Ljungemyr et al. 1996).

Below, some results of this simulation are described. The emphasis is on aspects of the model results that are either expected to be directly influenced by the land surface scheme or are important for understanding the behaviour of the simulated land surface parameters. The model results are naturally affected by other parameterizations as well. The present model version, denoted as RCA2, has undergone several changes from the original HIRLAM 2.5 code. Its predecessor, RCA1, was described by Rummukainen et

al. (2001) and already included the PROBE model and some changes in the soil and snow treatment. Since then, changes have also been made for clouds, convection and radiation. The new convection scheme is that due to Kain and Fritsch (1993). The large-scale cloud/condensation scheme is described in Rasch and Kristjánsson (1998). For vertical diffusion the CBR (Cuxart et al. 2000) scheme is used. The radiation scheme that originates from Savijärvi (1990) and Sass et al. (1994) has been modified to include an explicit CO_2 treatment (Räisänen et al. 2000), and a parameterisation of the effect of cloud heterogeneity and inhomogeneity on the short wave transmissivity of clouds. The latter mimics more detailed and models and observations indicating that short wave flux transmission through heterogeneous clouds exceeds that calculated by plane parallel clouds by about 20%. The present version of RCA2 has been embedded in the reference system of HIRLAM (version 4.7.4). It is described in some more detail by Jones (2001).

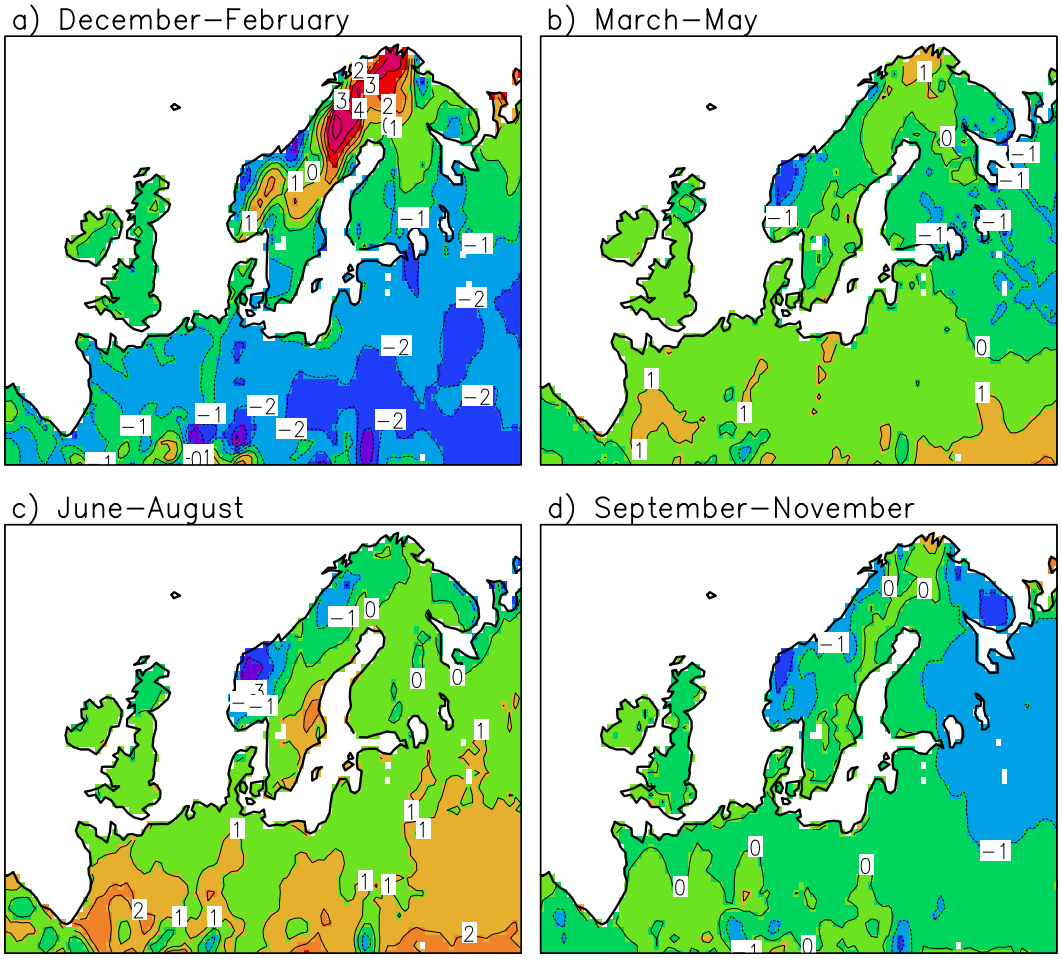

Figure 6. *Five-year seasonal mean differences (model minus CRU; in ºC) in height-adjusted two-meter temperature between the simulation and the CRU data set.*

The five-year monthly, seasonal and annual means discussed below are calculated over the period December 1988 – November 1993. The maps that are shown exclude, in addition to the 8-point boundary relaxation zones, the four outermost rows and columns of the ordinary model domain where some of the results (in particular, precipitation and cloudiness) are markedly affected by boundary zone spinup effects. Some of the results

are given as area means over the whole land area within this map domain (all grid boxes with at least 50% land cover), the Nordic region (land in Finland, Sweden, Norway and Denmark) or Sweden only. In the verification of the model results against observations, the CRU data set (Hulme et al. 1995; New et al. 1999, 2000) is mainly used.

Five-year seasonal mean biases in two-meter temperature are shown in Fig. 6. A simple adjustment is applied for differences in surface height between CRU data and model data assuming a constant lapse rate of 5.5ºC km^{-1}. The impact of this adjustment is generally small because the RCA2 and CRU orographies are close to each other.

The biases are generally relatively small, in wide areas within ±1ºC especially in autumn and spring. Areas and seasons of positive and negative bias more or less balance each other. In the southern half of the model domain, the simulated temperatures are somewhat too low in winter but slightly too high in summer. There is also a pronounced positive bias in northern Scandinavia in winter. Most of it may be real, but a part of it is likely to be explained by a local cold bias in the CRU data set. Most weather stations in this area are in valleys, which are in winter slightly colder than their environment (Raab and Vedin 1995). The CRU interpolation method cannot take this into account, since it treats height differences in a crude way, by assuming the same lapse rate (in winter about a 0.5ºC decrease in temperature for a 100 m increase in height) in the whole of Europe.

Winter and summer means of the average simulated and observed diurnal temperature range are shown in Fig. 7. The model generally underestimates the diurnal range in northern Europe, in particular during the warmer part of the year. In the Nordic area, the average diurnal range in summer is around 10ºC according to CRU, but only about 6ºC in the model. Towards the southern part of the domain, the simulated diurnal range in summer increases and more or less reaches the observed values. The difference between the southern and northern parts of the model domain is qualitatively as expected from the simulated total cloudiness (Fig. 9), which is, in summer, somewhat too high in northern Europe but too low near the southern boundary. The underestimation in northern Europe is also affected by subgrid scale lakes, which cover about 12% of the whole Nordic region. The lakes reduce the diurnal temperature range in the model output, which is, for each grid square, a weighted average over the land, water and ice fractions. By contrast, the CRU data set is based on observations from land stations. Finally, the simulated diurnal temperature range may be suppressed because the top layer temperature includes both upper soil and vegetation as discussed above.

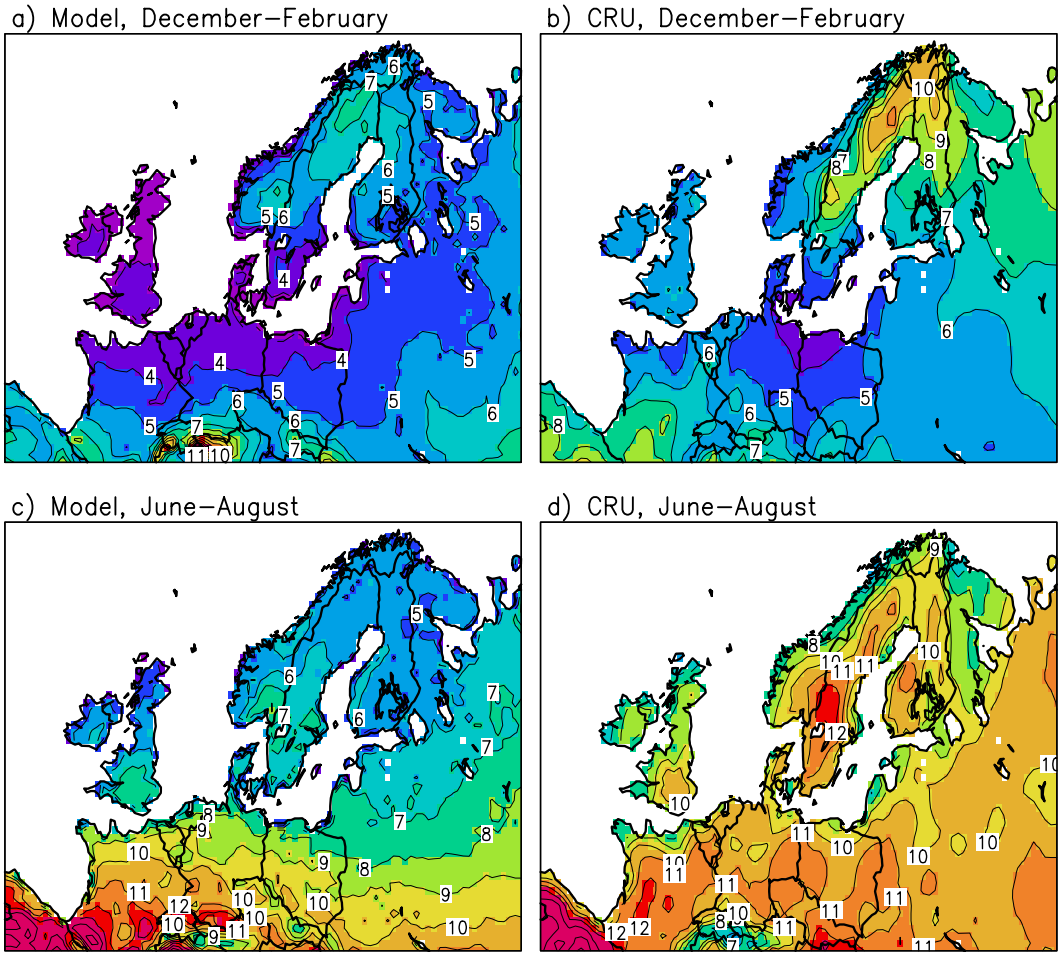

Figure 7. *Five-year seasonal mean diurnal temperature range (ºC) in the model (left) and according to the CRU data set (right) in winter (top) and summer (bottom). The maximum in northern Scandinavia in winter results from synoptic (rather than night-to-day) variability.*

The simulated 5-year mean annual precipitation is generally below the CRU precipitation estimate in the southern part of the model domain but generally above it in northern Europe (Fig. 8a-b). The difference for the whole Nordic region is +17% and that for Sweden +30%. These biases are, however, partly artificial, since the CRU data set is not corrected for measurement losses that are substantial particularly for solid precipitation. The larger area mean bias for Sweden is due to the fact that part of the orographic precipitation that in reality falls in Norway is transported over to northwestern Sweden in the model (note the dipole structure with negative biases in Norway and large positive biases in northwestern Sweden in Fig. 8b). This is most likely associated with the relatively low resolution and smooth orography in the model. More generally, the difference between the model and CRU tends to be most pronounced over high orography. Excluding areas above 500 m, the Nordic and Sweden mean differences are reduced to 10% and 23%, respectively.

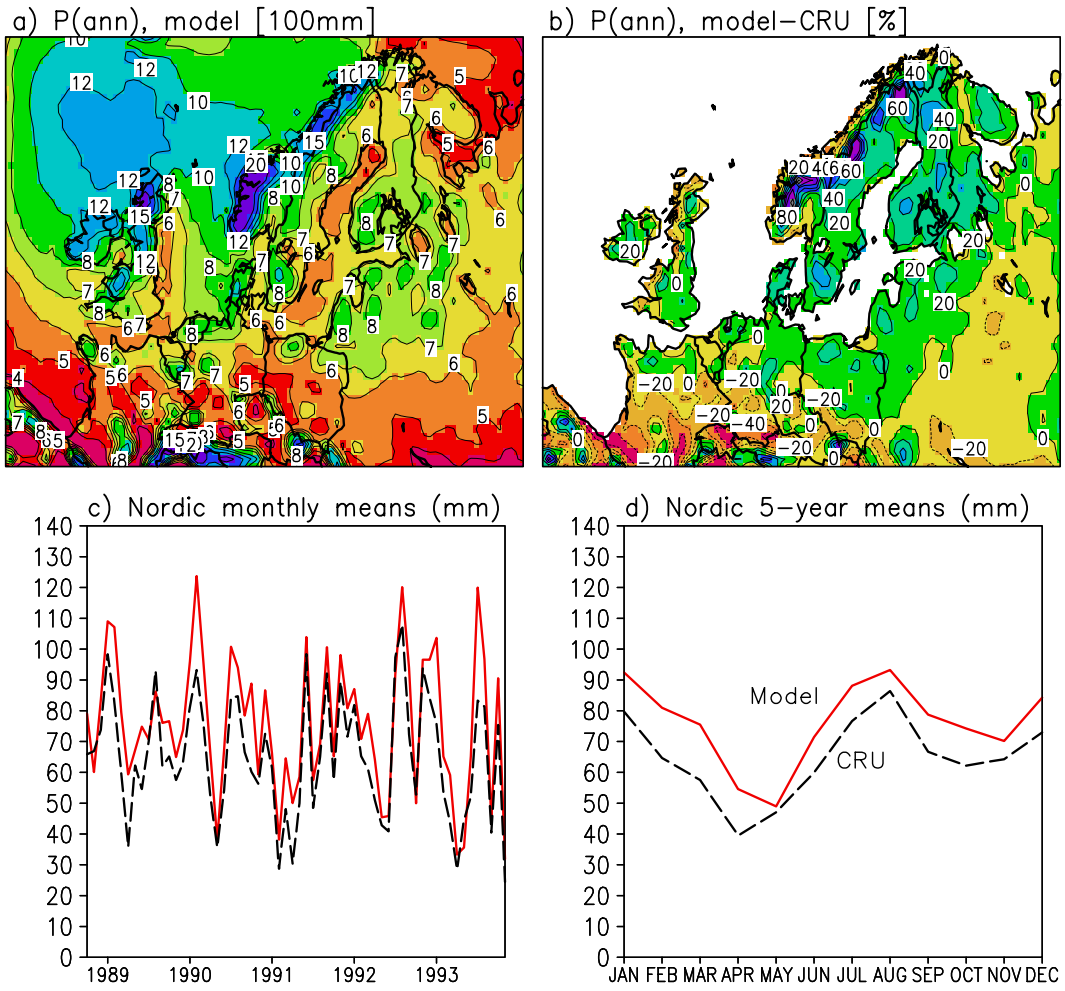

Figure 8. *(a) Five-year annual mean precipitation in the model (unit = 100 mm), (b) difference in annual precipitation between the model and the CRU data set (%), (c) monthly time series of Nordic mean precipitation in the model and according to CRU, and (d) the average seasonal cycles of the simulated and the CRU Nordic mean precipitation.*

As indicated by the Nordic means in Fig. 8c, interannual precipitation variability is generally captured well in the simulation. Disregarding the difference in annual means, the simulated average seasonal cycle is also in reasonable agreement with CRU (Fig. 8d).

Winter and summer means of the simulated total cloudiness and differences from the CRU cloudiness estimate for the same period are shown in Fig. 9. As noted above, the cloud cover in northern Europe is generally slightly more abundant in the model than according to the CRU data set (the difference in Nordic means is 6% of sky in winter and 8% in summer). Further south and west, total cloudiness is below the CRU estimate, with a somewhat larger difference in winter than in summer.

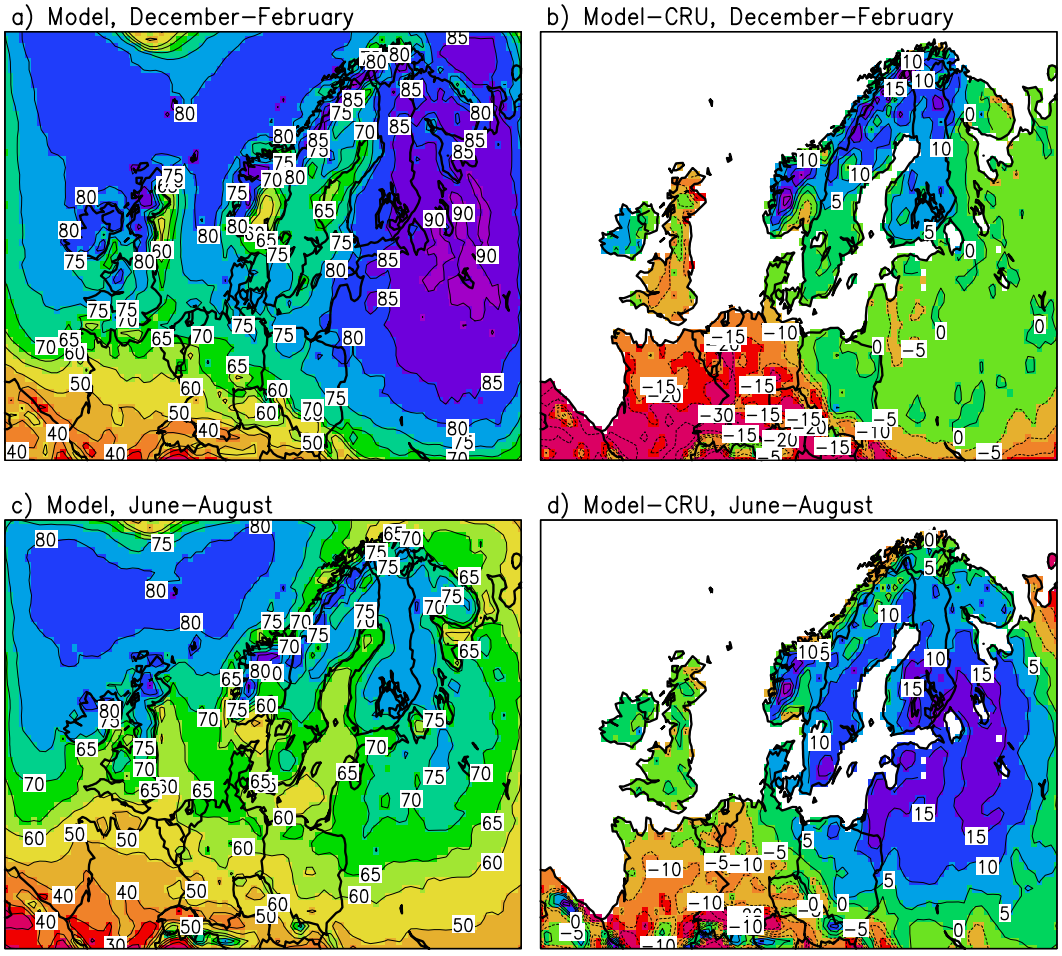

Figure 9. *Five-year mean simulated total cloudiness (%) in winter (a) and the difference from CRU (b); (c) and (d) as for (a) and (b), but in summer.*

The simulated 5-year mean 10-meter wind speed is shown in Fig. 10a. Wind data from CRU in Fig. 10b were only available for this study as a 30-year mean (1961–1990), which together with other problems with the observations (e.g., different measurement practices in different countries) complicates the comparison. In general, the simulated mean wind speeds are reasonably similar with the CRU ones. Some of the geographical patterns are also similar. In the Nordic region, the simulated wind speeds tend to exceed the CRU ones in winter (on the average by 19%) but are somewhat weaker than these in the other seasons (by up to 14% in summer). These features may, however, be affected by the difference in periods. In particular, the simulated five winters were all relatively mild with a positive phase of the North Atlantic Oscillation, which tends to lead to higher-than-average wind speeds in northern Europe in winter.

Five-year mean seasonal cycles of areally averaged (the whole land area, the Nordic region and Sweden) surface energy balance components are shown in Fig. 11. In northern Europe (i.e. for the Nordic region and for Sweden only), in particular, most of the net radiation is consumed by the latent heat flux in the warm season. Sensible heat flux is comparable with the latent heat flux only in April and May. This may be influenced by the relatively high total cloudiness discussed above, and it may itself

explain some of the underestimated diurnal temperature range. In individual rainfree days, though, the sensible heat flux may well be larger than the latent heat flux.

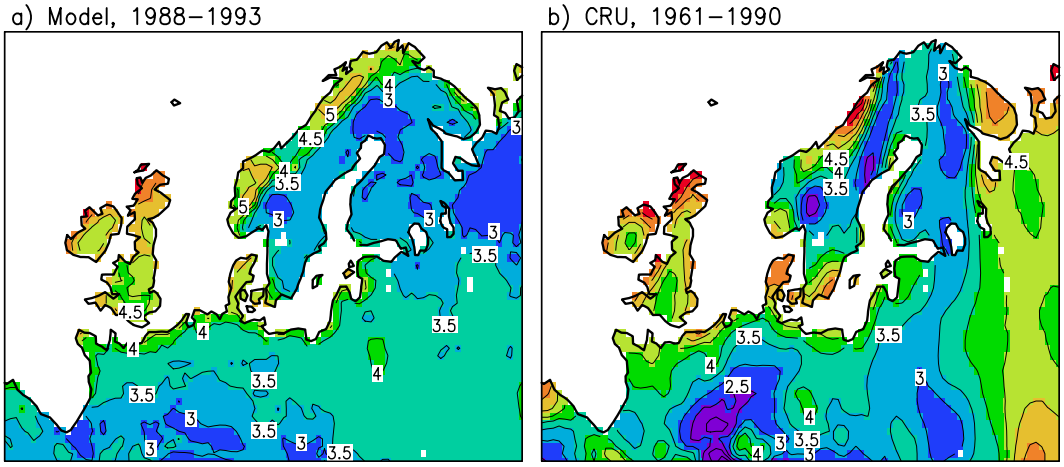

Figure 10. *Annual mean wind speed (m/s) (a) in the model in December 1988 – November 1993 and (b) according to the CRU data set in 1961–1990.*

In winter RCA2 simulates a rather large upward latent heat flux and a large downward sensible heat flux. The upward latent heat flux simulated for Sweden (with about 65 % forest as an area average in the database used) is equivalent to about 10 mm of evaporation per month (1 Wm^{-2} in *LE* equals about 1 mm per month in *E*). On the other hand, five winters of continuous eddy correlation measurements (described by Grelle and Lindroth 1996 and presented by Eklund et al. 2000) above a Swedish site dominated by forest show evaporation to be only 0-4 mm per month in December and January. However, these data may be uncertain, because they cover only one site. King and Connolley (1997) associate high simulated downward winter sensible heat flux with too small simulated downward longwave radiation. The introduction of an additional forest canopy air resistance, as described in Section 3.5, reduced winter evaporation only marginally.

One can also note from Fig. 11 that the net surface energy flux approximated here as $G = R_{net} - H - LE$ does not average out to zero in the annual mean. The annual mean value over the whole land area is 8 Wm^{-2}, or about 15% of the annual mean net radiation. In part, this is because the energy consumed by snowmelt has been neglected. This is estimated to be 1–1.5 Wm^{-2}, as averaged over the whole year and the whole land area. The remainder of the long-term mean net heat flux apparently derives from a cold bias in the prescribed (ERA) bottom soil temperatures. As averaged over the whole year and the whole land area, the ERA soil temperatures are about 1.2ºC colder than the 2 m air temperatures in RCA2 (despite the fact that the average bias in the latter is very close to zero), or 1.0ºC colder than the deep soil temperatures in RCA2.

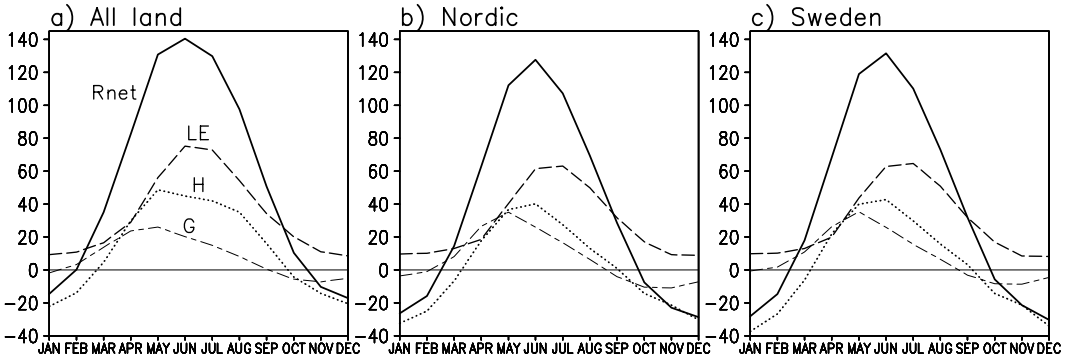

Figure 11. *Average seasonal cycles (Wm^{-2}) of surface net radiation (R_{net}), latent heat flux (LE), sensible heat flux (H) and heat flow to the soil ($G=R_{net}-H-LE$) in (a) the whole land area, (b) the Nordic region and (c) Sweden.*

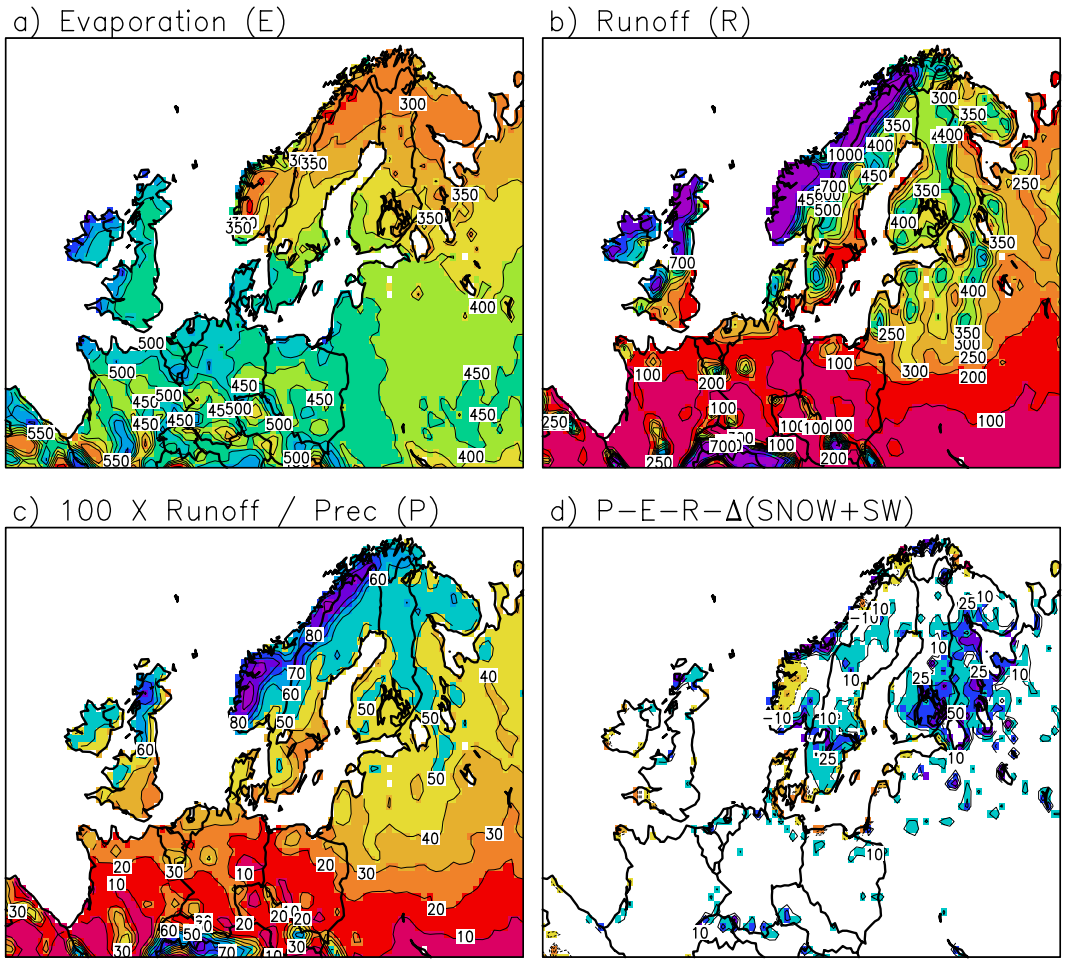

Figure 12. *Five-year means of (a) evaporation, (b) runoff, (c) the ratio between runoff and precipitation and (d) the numerical residual in the hydrological balance. Unit is mm/year in (a), (b) and (d) and per cent in (c). In (d), areas where the residual is within ±10 mm/year are left white.*

Mean annual precipitation was shown in Fig. 8. Other components of the surface water budget are given in Fig. 12. Evapotranspiration and runoff in Sweden appear to be, in general, reasonably well simulated in comparison with the 30-year mean (1961-1990) estimates presented by Raab and Vedin (1995). However, the simulated evapotranspiration in the northwestern part of the country clearly exceeds the observational estimate, shown in Fig. 13. Over much of central Europe, and to a lesser extent in southeastern Sweden, runoff generation is relatively small. Here, efficient evapotranspiration allowed by more radiative energy keeps the simulated soil moisture lower than further north (also recall that, in contrast with northern Europe, the simulated precipitation is too low in the southern part of the domain). This is further illustrated by the ratio between runoff and precipitation in Fig. 12c. Finally, over land surfaces, the difference *precipitation – evaporation – runoff* equals the change in soil moisture and snow, where the last term is relatively small when averaged over several years. As shown in Fig. 12d, this balance does not hold exactly in the model, but the unexplained numerical residual is within ±10 mm per year in most of the area. Larger values of the residual mainly occur at coasts and in lake-rich areas such as southeastern Finland, probably due to the fact that the grid square mean (land plus water fraction) evaporation in the model output may differ from the evaporation over land alone.

In northern Europe, over 40% of the annual total evapotranspiration comes from the evaporation of water intercepted on the vegetation canopy, as seen in Figs. 14a-b. The interception evaporation in Sweden has, like precipitation, a maximum in July-August whereas transpiration (which in summer constitutes most of the remaining evapotranspiration $E–E_R$) culminates a month earlier. These simulated features are considered to be largely occurring even in reality. Generally, the interception follows the rainfall amount and is larger for intermittent rainfall as showers than for rain falling more evenly in time. Comparison with Fig. 17 indicates that interception evaporation in Sweden in July – August is about 28% of the rainfall.

Fig. 15 shows five-year daily time series of soil moisture at four grid points. Here, the relative volumetric concentration of soil moisture in the two layers is shown; most of the absolute soil moisture amount resides in the thicker deep layer. For all four locations, the top soil layer is for most of the time moister than the deep layer, especially so in connection with precipitation events. During long dry periods, however, the top soil layer becomes the drier of the two due to the bare soil evaporation part E_G and the root extraction by transpiration E_{TRs}. This happens occasionally at all four locations but most frequently in the grid point in Spain. Here, the soil dries out more or less completely every summer, and even at the other three locations, summer deep layer soil moistures often decrease to less than a half of the winter value. The effect of the "beta-model" (Section 5.1) may be seen in the way that a certain precipitation-caused increase in the top layer soil moisture is reflected in the deep layer. The deep layer soil moisture shows less increase when this layer is already wet, compared with the situations when it is dry. This is so, because for a wet soil, more of the rainfall goes directly to runoff.

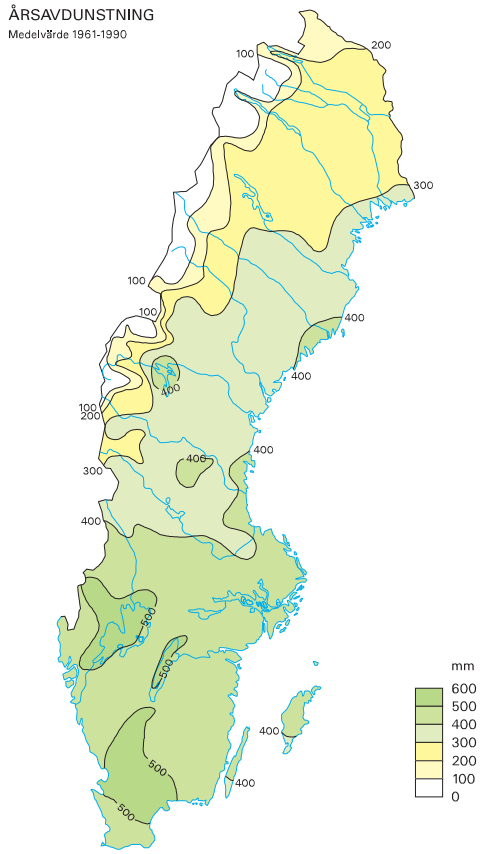

Figure 13. *Mean annual evaporation in Sweden during 1961-90 obtained as the difference between precipitation and runoff. From Raab and Vedin (1995).*

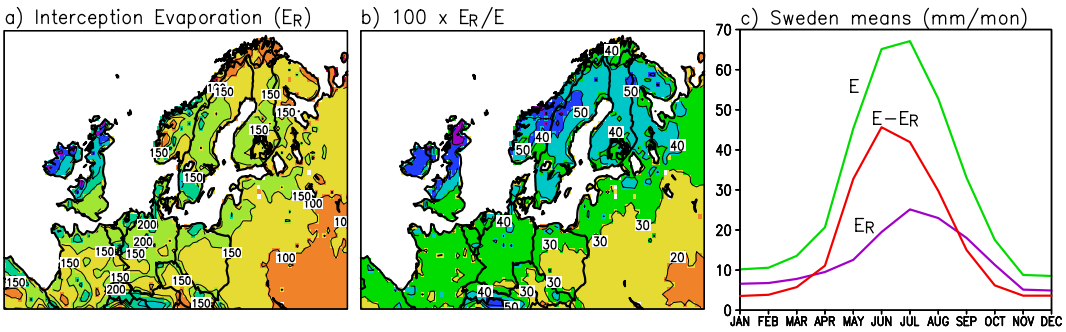

Figure 14. *(a) Five-year mean evaporation (mm/year) of intercepted water, (b) its fraction to total evapotranspiration (in per cent) and (c) the Sweden mean seasonal cycles (mm/mon) of the total evapotranspiration (E), the interception part (E_R) and the remainder ($E - E_R$ = sum of transpiration, bare soil evaporation and snow evaporation).*

The behaviour of the simulated snow cover, given in Fig. 16 as mm of water equivalent, appears intuitively reasonable, although no detailed verification against observations has been attempted. Examples of the daily time series of snow water equivalent in individual grid boxes are shown in the lower part of the figure. In the grid box in eastern Finland, a decent snow cover develops every winter and it typically survives to the end of April, which appears reasonably realistic. In southeastern Sweden, by contrast, only

sporadic snow cover is simulated in these predominantly mild winters. In the grid box over the western part of the Norwegian mountains, huge amounts of snow fall in every winter. The snow remains on the ground to the late summer but, excluding the year 1993 with exceptionally large winter snowfall, it nevertheless melts completely before the new snowfall season commences in the autumn.

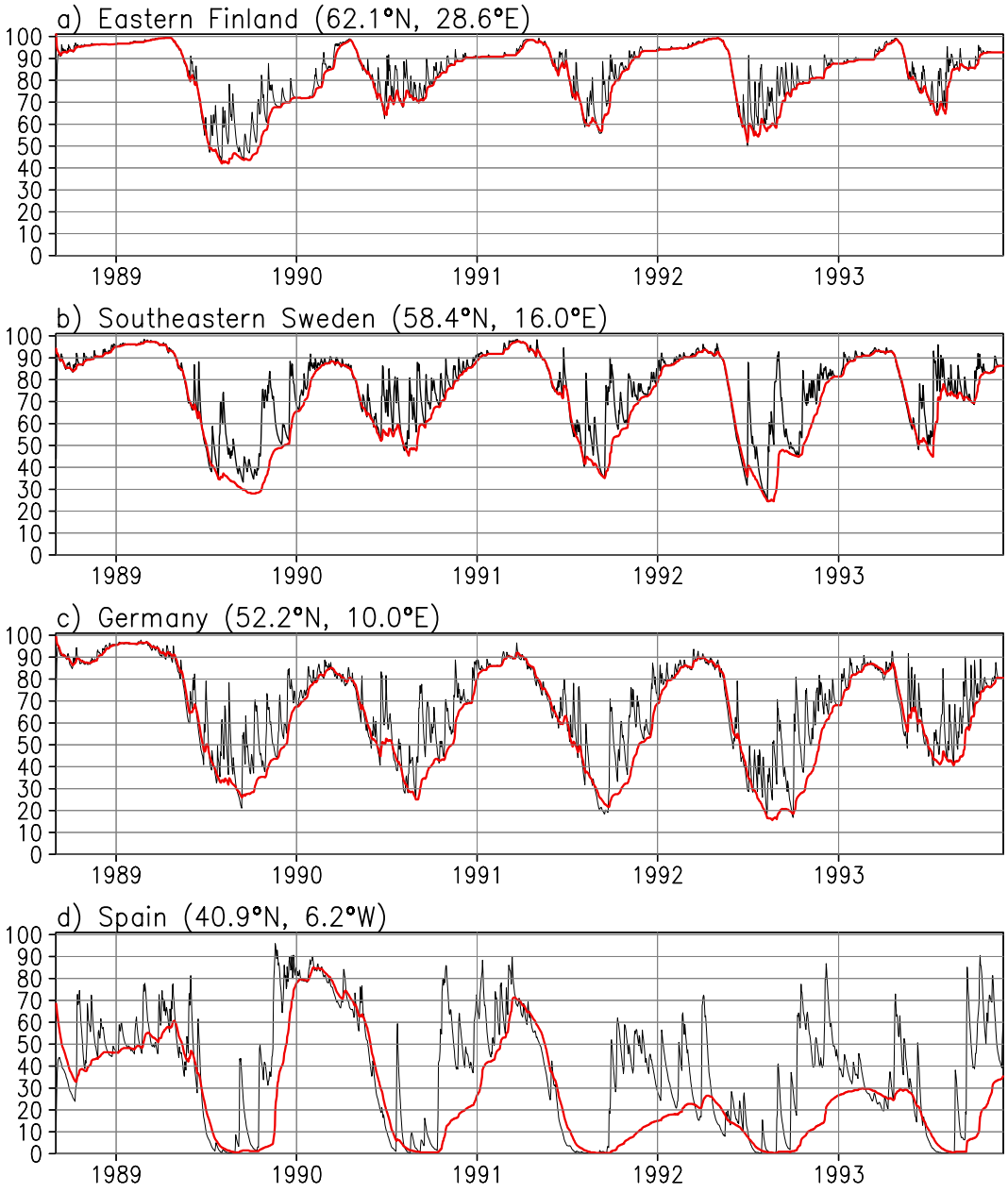

Figure 15. *Daily time series of soil moisture at four grid points. Soil moisture is given in per cent of field capacity for the top soil layer (black curves) and the deep soil layer (red curves). The field capacity corresponds to 20 mm of water in the top soil layer and 20 × 0.8/0.072 = 222 mm in the deep soil layer, making up a total of 242 mm of water in the two layers.*

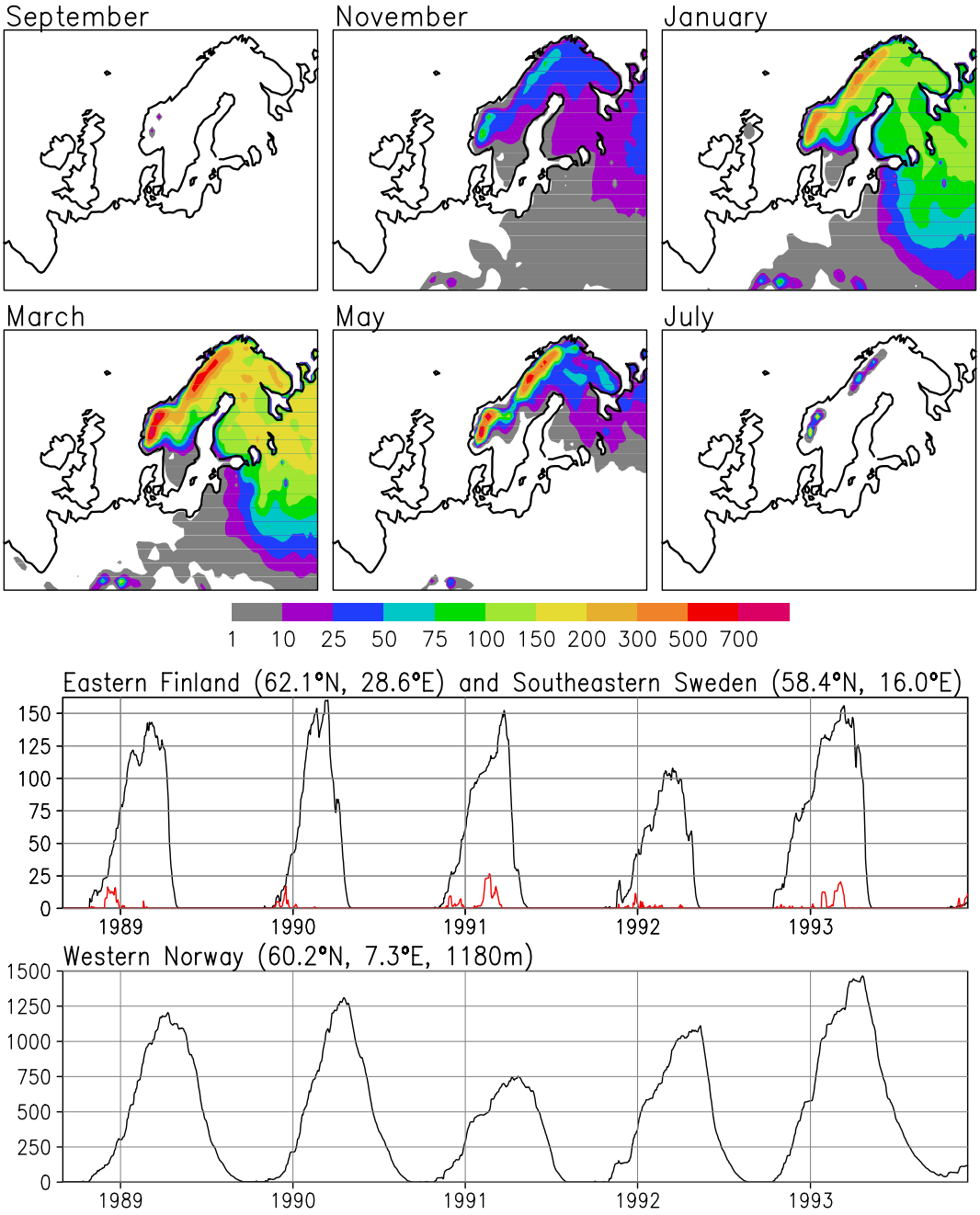

Figure 16. *Top two rows: five-year means of snow water equivalent (in mm of water) in some calendar months. Third row: daily time series of snow water equivalent in eastern Finland (black) and southeastern Sweden (red). Bottom: daily time series of snow water in a grid point in western Norway (note the difference in scale).*

Fig. 17 summarizes the area mean hydrology for Sweden. The five-year average annual precipitation is similar to that for the Nordic area shown in Fig. 8. Runoff shows a maximum in spring due to snowmelt and is reduced in summer due to the evapotranspiration loss. The completely snow-free period in summer is short, because

the area mean includes the northern and mountainous parts of the country where snow melts late in the spring and comes early in the autumn.

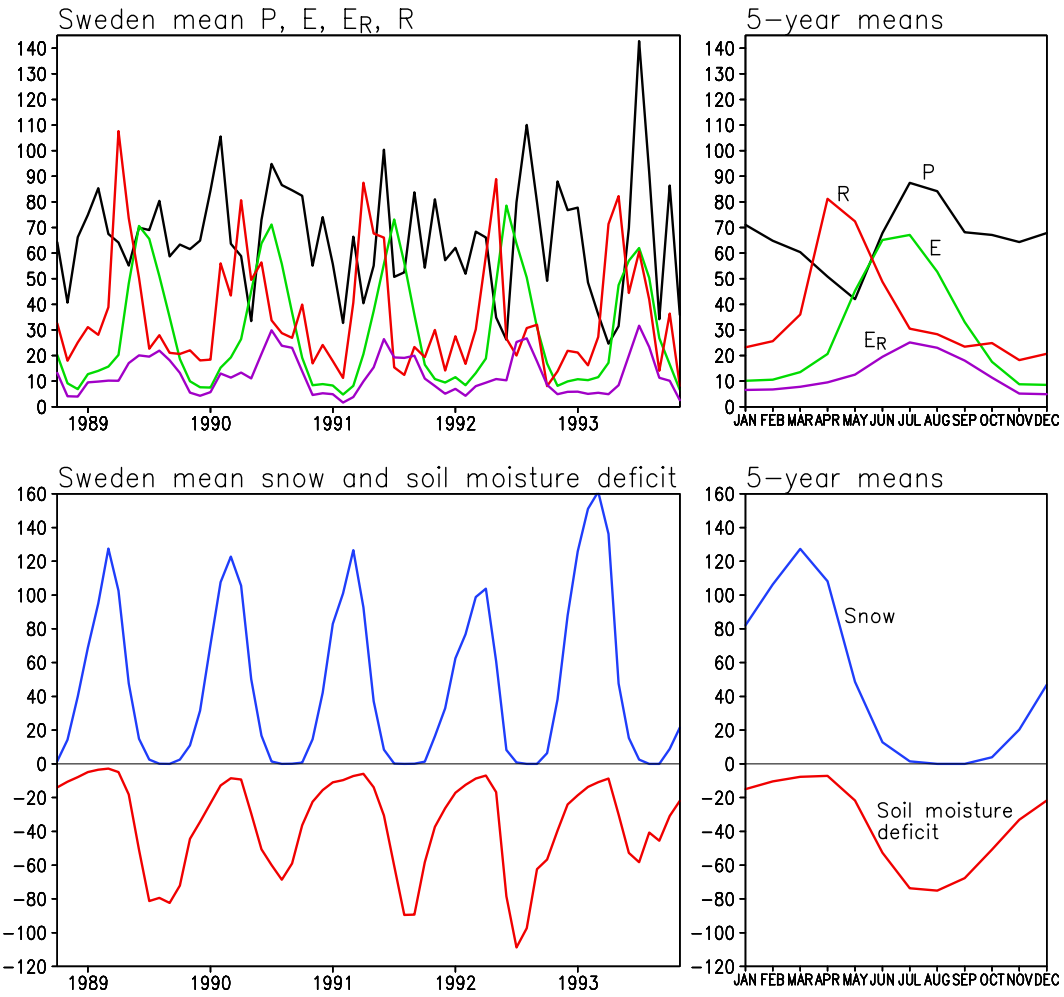

Figure 17. *Simulated Sweden area mean hydrology. Top: precipitation (P), evapotranspiration (E), evaporation of intercepted rainfall (E_R) and runoff (R) in each simulated month (left) and the average annual cycle (right). Bottom: Snow water equivalent and soil moisture deficit (in mm; summed over both layers).*

15 Summary and discussion

A previous HIRLAM surface treatment, used in operational weather forecasting, has been expanded to include,

1) Modifcations of the ISBA model for vegetation transpiration and rainfall interception;
2) Processes based on hydrological experience for treatment of soil moisture, runoff and snow;
3) A model for hydraulic and thermal soil properties that depend on soil moisture and a geographical field of soil texture.

Improvements had to be made concerning many other aspects such as numerical performance and compatibility with the HIRLAM framework. As in the original HIRLAM version, only one surface temperature has been used for simulating top soil layer, vegetation canopy and partial or full snow cover.

As in the original HIRLAM version, surface temperature may exceed 0ºC even for a full snow cover on a land surface. This simulates surfaces which may be above zero degrees such as houses, trees etc. However, there are limitations to the rise of surface temperature such as the consumption of energy for snowmelt and a higher snow albedo.

As in previous HIRLAM versions, soil temperatures are described by two layers of depth 0.072 m and 0.432 m and a bottom climatological layer relaxed to temperatures from ERA or a GCM. The introduction of the hydrological soil moisture/runoff model implied that no relaxation should be made for soil moisture. Consequently, to maintain a reasonably large maximum total soil water content, the deep soil layer depth had to be increased (to 0.8 m). The improvements to vegetation effects (transpiration, interception) are important for describing feedback effects between atmosphere and vegetation.

Suggested future improvements and additions to the present land-surface treatment include the following:

- improved calculation of the momentum, latent heat and sensible heat fluxes at the earth surface by revising stability functions in very stable situations (e.g., by using the formulation of Zilitinkevich and Calanca 2000) and by separating the roughness lengths for momentum and heat;
- inclusion of separate temperatures for snow and vegetation;
- use of geographical fields for more vegetation parameters such as the leaf area index;
- a parameterization of the subgrid-scale variability of rainfall and its interception.

In addition, the land surface climate depends on the radiation components reaching the earth surface, the vertical diffusion scheme, the stability functions and on other parts of the physics parametrization.

Nevertheless, as discussed in the previous section, even the current model version gives in many respects reasonable results when driven by ERA boundary data. In the five-year three-dimensional model run conducted, RCA2 with the present land surface scheme suffers only relatively modest biases in average two-meter temperature, even though the diurnal temperature range is somewhat small in northern Europe. Agreement between simulated and analysed (CRU) precipitation in northern Europe is reasonable (Fig. 8), in particular considering the likely negative bias in the latter.

The variations and magnitudes of snow cover, soil moisture and interception evaporation all showed to be realistic. As a numerical check, the overall water balance during the five years simulated was seen to be well satisfied, which is a prerequisite for

adequate performance of the model. Annual evapotranspiration in Sweden (Fig. 12) is in fair agreement with a 30-year estimate, although with apparently somewhat too high fluxes in northern Sweden. In winter, however, the upward latent heat flux is substantially larger than indicated by long-term eddy correlation measurements above a forest in Sweden, and the downward sensible heat flux also appears to be overpredicted by the model.

Acknowledgements

Michael Tjernström, Colin Jones, Markku Rummukainen, Patrick Samuelsson, Sten Bergström, Marie Gardelin and Lars Moen have given valuable help and comments. Ulf Hansson has taken part in preparing the model code.

References

Arpege-Climat 1996. Modelisation Communautaire. I. Documentation algorithmique, Version 2. Météo-France, 12 Janvier 1996.

Bergström S. 1976. Development and application of a conceptual runoff model for Scandinavian catchments. SMHI Reports RHO, No. 7, Norrköping.

Bergström S. 1990. Parametervärden för HBV-modellen i Sverige. (Parameter values in the HBV model in Sweden, in Swedish). SMHI, Rapporter Hydrologi, Nr 28, Swedish Meteorological and Hydrological Institute, 35 pp.

Bergström S. 1995. The HBV Model. In: V.P. Singh (Ed.), Computer Models of Watershed Hydrology. Water resources Publications, Highlands Ranch, Colorado, pp. 443-476.

Bringfelt B., Gustafsson N., Vilmusenaho P. and Järvenoja S. 1995. Updating of the HIRLAM physiography and climate data base. HIRLAM Technical Report No. 19. Norrköping, June 1995.

Bringfelt B., Heikinheimo M., Gustafsson N., Perov V. and Lindroth A. 1999. A new land-surface treatment for HIRLAM – comparisons with NOPEX measurements. Agricultural and Forest Meteorology 98-99, 239-256. NOPEX Special Issue.

Clapp R.B. and Hornberger G.M. 1978. Empirical equations for some hydraulic properties. Water Resources Research, 14, 601-604.

Cuxart J., Bougeault P. and Redelsperger J.-L. 2000. A turbulence scheme allowing for meso-scale and large-eddy simulations. Quart. J. Roy. Met. Soc., 126, 1-30.

Douville H., Royer J.-F. and Mahfouf J.-F. 1995. A new snow parameterization for the Météo-France climat model. Climate Dynamics, 12, 21-35.

Eerola K. 1996. Experiences with the analysis of sea surface temperature, ice coverage and snow depth. HIRLAM 3 Workshop on soil processes and soil/surface data assimilation. Norrköping, February. 1996.

Eklund A., Gardelin M. and Lindroth A. 2000. Vinteravdunstning i HBV-modellen – jämförelse med mätdata. (Winter evaporation in the HBV model - comparisons with measuring data, in Swedish). SMHI, Hydrologi Nr 83.

FAO-Unesco 1981. Soil map of the world: Vol. 5, Europe. Unesco-Paris, 91 pp.

Gibson J.K., Kållberg P., Uppala S., Hernandez A., Nomura A. and Serrano E. 1997. ERA description. ECMWF Reanalysis Project Rep. Series 1, European Centre for Medium Range Weather Forecasts, Reading, United Kingdom, 66 pp.

Gollvik S. and Olsson E. 1995. A onedimensional interpretation model for detailed short range forecasting. Meteorological Applications, 2, 209-216.

Gray D.M. and Male D.H. (eds.) 1981. Handbook of snow. Toronto, 776 pp.

Grelle A. and Lindroth A. 1996. Eddy-correlation system for long-term monitoring of fluxes of heat, water vapour and CO_2. Global Change Biology, 2, 297-307.

Hagemann S., Botzet M., Dümenil L. and Machenhauer B. 1999. Derivation of global GCM boundary conditions from 1 km land use satellite data. Report No. 289. Max-Planck-Institut für Meteorologie, Hamburg.

Hulme M., Conway D., Jones P.D., Jiang T., Barrow E.M. and Turney C. 1995. Construction of a 1961-1990 European climatology for climate change modelling and impact applications. International Journal of Climatology, 15, 1333-1363.

Jones C. 2001. A brief description of RCA2 (Rossby Centre Atmosphere Model version 2). SWECLIM Newsletter, 11, in press.

Kain J.S. and Fritsch J.M. 1993. Convective parameterization for mesoscale models: the Kain-Fritsch scheme. The Representation of Cumulus in Numerical Models. Meteorological Monographs, Emanuel and Raymond Eds., 24,165-170.

King J.C. and Connolley W.M. 1997. Validation of the Surface Energy Balance over the Antarctic Ice Sheets in the U.K. Meteorological Office Unified Climate Model. Journal of Climate, 10: 1273-1287.

Källén E. (Editor) 1996. HIRLAM Documentation Manual. System 2.5.

Lindström G., Gardelin M., Johansson B. and Bergström S. 1997. Development and test of the distributed HBV-96 hydrological model. Journal of Hydrology, 201, 272-288.

Lindström G. and Gardelin M. 1999. A simple snow parametrisation scheme intended for the RCA model based on the HBV runoff model. SWECLIM Newsletter No. 6.

Ljungemyr P., Gustafsson N. and Omstedt A. 1996. Parameterization of lake thermodynamics in a high resolution weather forecasting model. Tellus, 48A, 608–621.

Louis J. F., Tiedtke M. and Geleyn J.F. 1982. A short history of the operational PBL-parametrization at ECMWF. Workshop on boundary layer parametrization, Nov. 1981, ECMWF, Reading, England.

Mason P.J. 1988. The formation of areally-averaged roughness lengths. Quarterly Journal of the Royal Meteorological Society, 114, 399-420.

McCumber M. and Pielke R. 1981. Simulation of the effects of surface fluxes of heat and moisture in a mesoscale numerical model. I. Soil layer. Journal of Geophysical Research, 86, 9929-9938.

Meier H.E.M., Döscher R., Coward A.C., Nycander J. and Döös K. 1999. RCO – Rossby Centre regional Ocean climate model description (version 1.0) and first results from the hindcast period 1992/1993. SMHI Reports Oceanography No. 26, 101 pp.

Morén A.-S., Lindroth A., Flower-Ellis J.G.K., Cienciala E. and Mölder M. 2000. Branch transpiration of pine and spruce scaled to tree and canopy using needle biomass distributions. Trees, 14, 384-397.

New M., Hulme M. and Jones P. 1999. Representing twentieth-century space-time climate variability. Part I: Development of a 1961-90 mean monthly terrestrial climatology. Journal of Climate, 12, 829-856.

New M., Hulme M. and Jones P. 2000. Representing twentieth-century space-time climate variability. Part II: Development of 1901-96 monthly grids of terrestrial surface climate. Journal of Climate, 13, 2217-2238.

Noilhan J. and Planton S. 1989. A simple parametrization of land surface processes for meteorological models. Monthly Weather Review, 117, 535-549.

Raab B. and Vedin H. (Special editors) 1995. Climate, Lakes and Rivers. National Atlas of Sweden. Available from SMHI, S-60176 Norrköping, Sweden.

Rasch P.J. and Kristjánsson J.E. 1998. A comparison of the CCM3 model climate using diagnosed and predicted condensate parameterizations. Journal of Climate, 11, 1587-1614.

Rummukainen M. 1999. On the movement of soil water: "Under what conditions may water flow upwards?" SWECLIM Newsletter No. 4, SMHI, Norrköping.

Rummukainen M., Räisänen J., Ullerstig A., Bringfelt B., Hansson U., Graham P. and Willén U. 1998. RCA - Rossby Centre regional Atmospheric climate model: model description and results from the first multi-year simulation. SMHI, RMK No. 83, 76 pp.

Rummukainen M., Räisänen J., Bringfelt B., Ullerstig A, Omstedt A., Willén U, Hansson U. and Jones C. 2001. A regional climate model for northern Europe: model description and results from the downscaling of two GCM control simulations. Climate Dynamics, 17, 339-359.

Räisänen, P., Rummukainen M. and Räisänen J. 2000: Modification of the HIRLAM radiation schemre for use in the Rossby Centre regional atmospheric climate model. Report No. 49, Department of Meteorology, University of Helsinki, 71 pp.

Sass B.H., Rontu L. and Räisänen P. 1994. HIRLAM-2 Radiation Scheme: Documentation and Tests. HIRLAM Technical Report No. 16, Norrköping, 43 pp.

Savijärvi H. 1990. Fast radiation parameterization schemes for mesoscale and short-range forecast models. Journal of Applied Meteorology, 29, 437-447.

Schmugge J. and André C. (editors) 1991. Land Surface Evaporation. Measurement and Parameterization. Springer Verlag.

Van den Hurk B., Viterbo P., Beljaars A. and Betts A. 2000. Offline validation of the ERA40 surface scheme. ECMWF Technical memorandum No. 295.

Viterbo P. 1996. The representation of surface processes in general circulation models. PhD-thesis, 201 pp. Univ. Lisbon, January 1996 (ECMWF report of January 1996).

Viterbo P., Beljaars A., Mahfouf J.-F. and Teixeira J. 1999. The representation of soil moisture freezing and its impact on the stable boundary layer. Quarterly Journal of the Royal Meteorological Society, 125, 2401-2426.

Zilitinkevich S. and Calanca P. 2000. An extended similarity theory for the stably stratified atmospheric surface layer. Quarterly Journal of the Royal Meteorological Society, 126, 1913-1923.

SMHI

Swedish Meteorological and Hydrological Institute
SE 601 76 Norrköping, Sweden.
Tel +46 11-495 80 00. Fax +46 11-495 80 01

ISSN 0347-2116